ACCOUNTING FOR VARIATIONS IN THE SPECTRAL IRRADIANCE DISTRIBUTION IN PV PANEL PERFORMANCE MODEL

February 16, 2013

Bart van Dam

Energy science research project

University Utrecht

Supervised by Dr. W.G.J.H.M. van Sark & B. Elsinga, MSc

ABSTRACT

Photovoltaic (PV) panel performance is strongly influenced by the available incident irradiance and the module temperature. Since these conditions vary on different timescales, the actual outdoor energy yield of PV modules is hard to anticipate. Diode models exist, correcting for total irradiance and temperature variations, which are able to accurately predict the outdoor performance of crystalline-silicon (c-Si) modules. The performance of amorphous-silicon (a-Si) photovoltaic modules, however, is mainly affected by the spectral distribution of the incident light, which is not included in most PV performance models. With the increasing market share of amorphous silicon, the need to include spectral information is growing. Accommodating variations in the spectral irradiance to improve PV performance models on clear days in the Netherlands is investigated in this report. For this, three spectral characterization methods are examined: the total irradiance, the useful irradiance and the average photon energy of the spectrum. Daily variations in the spectral irradiance are revealed by the useful irradiance and average photon energy; whereas the spectral effects on PV performance stress that the total irradiance is not sufficient for characterization of the incident irradiance for PV performance modeling. Additionally, it is shown that the spectral distribution has only a small effect on crystalline-silicon panel performance modeling. Of the three spectral parameterization methods investigated, the useful irradiance shows best results in accounting for the spectral irradiance on clear days and the modeling accuracy for amorphous-silicon modules can be improved significantly. However, low modeling accuracy is obtained at low incident irradiance, which is caused by a blue shift of the spectrum, not captured by the useful irradiance. The average photon reveals these changes; nevertheless on clear days, a simple relation between module performance and APE to correct for these spectral changes was not found. Improving PV performance modeling under low irradiance remains a challenge and requires more comprehensive characterizations of the spectral irradiance than the average photon energy and useful irradiance.

ACKNOWLEDGEMENTS

First of all I would like to thank Wilfried van Sark for providing me with a great research project. The topic is relevant, has direct applications and embraces both physics and programming, which greatly connect to my personal interests and background. During this research, my interest in photovoltaics has increased even more.

Secondly, thanks to Bo Burgmans, for sharing his knowledge on spectral modeling and pointing out the errors contained in the experimental dataset. This truly gave me a head start in my project.

Also, my gratitude goes to Alexander Los for granting permission to use data from the experimental setup of EKO Instruments Europe. Without this data, model validation and consequently this entire research would not have been possible.

Last but not definitely not least, I would like to thank Boudewijn Elsinga for all the useful discussions we had and his suggestions for my research. Also for his support and introductory assignments for Wolfram Mathematica, allowing me to quickly familiarize with the program.

TABLE OF CONTENTS

1. INTRODUCTION

1.1. JUSTIFICATION

Within the field of energy science, the main focus shifts towards renewable energy. Clean and abundant energy sources can provide the alternative to the conventional, environmentally intensive, fossil fuels. Among renewable energy technologies, photovoltaic (PV) power production shows great potential due to the rapid technological improvement in harvesting the large amount of energy contained in the sun's irradiation.

PV solar energy does, however, have disadvantages compared to fossil fuels. The main issue being that the performance of PV panels depends on the availability of incident solar irradiation. This is in contrast with conventional power plants, which can produce a specified amount of electricity whenever needed. Since irradiation on a panel can vary significantly on different timescales, the actual power output of a PV panel is hard to anticipate and is not constant. Rated performance data that is supplied by the manufacturer usually applies to Standard Test Conditions (STC, i.e. irradiance of 1000 W/m^2, ASTM G-173 standard spectrum and module temperature of 25°C) only and does rarely apply to non-ideal real-life conditions, e.g. variations in spectrum and module temperature. Still, it is of importance to be able to forecast the produced power of a PV system, for the implementation on different scales. On a small residential scale, the choice for the most cost efficient PV module depends on its outdoor energy yield; on large scales, grid operators and utility companies need to anticipate the variability in performance of a large PV plant or network to determine the back-up capacity that is required to produce a constant output. Overestimation of the variability leads to overcompensation and therefore higher costs (Hoff & Perez, 2012)[1].

On the scale of individual panels, there is a wide variety of models available, both for modeling incident irradiation (Demain, Journée, & Bertrand, 2012) (Badescu, et al., 2012) and for modeling the corresponding PV performance. The latter range from empirical models, to single-diode models to more complex and computationally intensive, two-diode models. Crystalline silicon (c-Si) solar panels are mainly affected by the module temperature (Minemoto, et al., 2007), which can be modeled accurately. The performance of amorphous silicon (a-Si) modules however is dominated by spectral effects, i.e. shift in the photon energy distribution of incident irradiation, which are not included in most models as they can be neglected for crystalline cells (Minemoto, et al., 2007). For multi-junction thin film solar cells spectral shift is expected to have an even more dominant effect on the performance (Krishnan, et al., 2009). With the increasing market share of amorphous silicon and thin film modules, the importance to model spectral effects thus grows.

1.2. SCOPE & RESEARCH QUESTION

Recently, researchers of the Copernicus[2] institute and Debye[3] Institute of the University Utrecht have designed and built a PV test installation (UPOT) to investigate spectral effects and module performance (van Sark, Louwen, de Waal, Elsinga, & Schropp, 2012). Located on the Hans Freudenthal building at

[1] PV plants and networks of PV systems combined with smart grids require even more detailed information on the energy yield of individual parts of the system. Smart grids are designed to flatten out the peak demand by switching appliances on when there is cheap excess energy production. For this, high temporal resolution data on energy demand and supply is required. Since the power output of PV panels can be strongly variable on different timescales e.g. due to transit clouds, incorporation of PV electricity generation in smart grids faces problems.

[2] Utrecht University, Copernicus Institute of Sustainable Development.

[3] Utrecht University, Debye Institute for Nanomaterials Science, Physics of Devices.

the Uithof in Utrecht, the test installation will measure the performance of 12 different commercially available PV modules and the corresponding environmental conditions, e.g. spectral irradiance, cloud coverage, module temperature etc. This information allows, among others, spectral variations to be correlated with Dutch weather conditions. Besides, correlation between PV performance, of in particular a-Si, and spectral irradiance distribution can be investigated.

This research will be conducted in the framework of the latter; Results will supplement those of the UPOT when it is operational. Since the geographical location of the UPOT is representative for Dutch weather conditions this research will be scoped to Dutch environmental conditions. The research question and sub questions yield:

- ***How can variations in the spectral irradiance distribution be accommodated to improve photovoltaic module performance modeling under Dutch outdoor conditions?***

- *How can changes in the spectral irradiance distribution be characterized?*
- *Does inclusion of spectral irradiance characterizations improve the accuracy of a-Si and c-Si panel performance models compared to conventional models?*

Additionally, the scripts[4] of the models that are analyzed during this research will be available to the solar energy group at the Copernicus institute. These PV models can contribute to a generic multi-parameter PV performance model that can predict the photovoltaic energy yield based on environmental conditions and module specific parameters.

1.3. RESEARCH OUTLINE

A full PV performance model is schematically depicted in Figure 1. It consists of a part that obtains and characterizes the environmental conditions and a second part that simulates the PV module under these conditions. PV modules are influenced by three environmental parameters: The module temperature, T, total incident irradiance, G and the spectral distribution of the irradiance E(λ), which is a function of wavelength. Additionally, optical effects such as shading and angle of incidence affect PV performance (Betts, 2004).

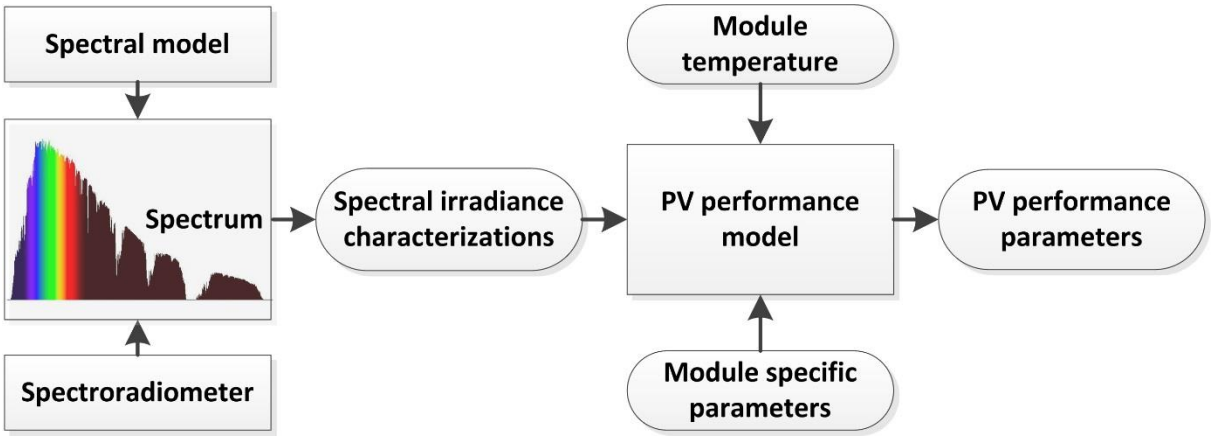

Figure 1 Schematic representation of the steps involved in modeling the performance of a PV module under outdoor conditions. Environmental conditions that influence solar panels are module temperature and (spectral) irradiance. Additionally, module specific parameters serve as input to the PV performance model. Atmospheric and environmental parameters, such as aerosol concentration, cloud coverage etc., serve as input to the spectral model (Myers, 2012).

[4] Created using Wolfram Mathematica 8.0.

The total irradiance is for the energy yield of both a-Si and c-Si of major importance. Current in the semiconductor material is induced by exposure to light, which determines the performance to a large extent. Besides G, the performance of c-Si modules is mainly affected by temperature variation. Increased module temperature enhances carrier generation and consequently recombination within the cell. As a result, the open circuit voltage decreases and the generated power is reduced (Twidell & Weir, 2006). Amorphous silicon based panels, however, suffer less from temperature changes and are mainly affected by variation in the spectral distribution (Minemoto, et al., 2007).

Temperature variations are accounted for in most PV panel models, by means of temperature coefficients that are often supplied by the manufacturer[5]. Spectral effects, however, lack a comprehensive classification. Chapter 2 therefore elaborates on the characterization methods of spectral irradiance that are used in this research. It is hereby assumed that the incident spectrum is known, obtained either by measurements with a spectroradiometer or by means of modeling. This assumption follows from the fact that multiple accurate spectral models are readily available, such as SMARTS2 (Gueymard, 2001) and SPECTRAL2 (Bird & Riordan, 1986) and more complex such as SEDES2 and TMYSPEC (Myers, 2012). Atmospheric composition, cloud coverage and angle of incidence are key parameters in spectral modeling.

For the performance model in Figure 1, a wide variety of PV performance models exist, of which two types will be discussed and presented in chapter 3: a simple two-diode model and an empirical model. Diode models are commonly used for c-Si performance modeling and will here be used as modeling benchmark. Moreover, the diode model will demonstrate the flaws of modeling the performance of a-Si modules. The empirical model accounts for variations in the spectral irradiance and is hence expected to perform better for a-Si modules. Both models will be analyzed and validated for both a-Si and c-Si type modules under outdoor conditions, in chapter 6. Experimental data on four different panels, provided by EKO Instruments Europe located in The Hague, will be used for model validation. This data set is presented and examined in chapter 4.1 and 5 respectively. In the final chapters, the modeling accuracy of the empirical model is compared to the accuracy of the two-diode model and these results are discussed.

[5] See chapter 3.1.

2. CHARACTERIZING THE SPECTRAL IRRADIANCE

A photovoltaic module harnesses the energy of the sun by converting incident photons into direct current. The number of available photons and their energy are therefore key parameters in PV performance modeling. A spectrum contains this information; to illustrate this, the reference spectrum under standard test conditions is shown in Figure 2. Most PV performance models however don't utilize all the spectral information as input as this is far too detailed and processing all the data points is time consuming. More conveniently, a single parameter is used to characterize the incident light. Three commonly used characterization methods are discussed here. PV performance models will be assessed based on these different characterization methods.

2.1. TOTAL INTEGRATED IRRADIANCE

Total irradiance, denoted by G, equals the total energy content of the spectral irradiance, i.e. $G = \int E(\lambda) d\lambda$, where $E(\lambda)$ is the spectral irradiance per unit area for wavelength, λ. Total irradiance is most commonly used in PV performance rating and modeling and can be obtained e.g. from meteorological observatories such as that of the Royal Netherlands Meteorological Institute (KNMI). The total irradiance, however, does not contain information on energy of individual photons; it does not distinguish between G obtained by many low energy photons and G obtained by a few high energy photons. Figure 2 shows the ASTM G1-73 standard spectrum and the corresponding total irradiance, represented by the graph's total surface.

2.2. USEFUL IRRADIANCE

Depending on the semiconductor material used, a PV module is sensitive only to part of the incident photons. On the one hand, the band gap energy, E_g, sets the lower limit for the photon energy, required to contribute to the photo current in the cell. On the other hand, high energy photons are mostly reflected at the air-module interface or absorbed in the front cover glass. These effects are captured in detail by the external quantum efficiency (EQE)[6]. The EQE gives as a function of photon wavelength, the ratio of the number of charge carriers that are generated in the solar cell to the number of incident photons on the module. Since module EQE is not commonly available, a first order correction to the total irradiance can be defined as the useful irradiance, $UI = \int_a^b E(\lambda) d\lambda$. This relation considers only part of the incident irradiance to which the PV module is sensitive. Below the lower limit a, the EQE equals zero, caused by reflectance of short wavelength photons; the upper limit, b, is set by the cut-off wavelength related to the band gap of the semiconductor material. The UI implicitly approximates the EQE with a step-function. Photons with energy below the direct band gap have $EQE_{E<E_g} = 0$. The external quantum efficiency of high energy photons with wavelength between a and b is set to 1 (Gottschalg, Betts, Infield, & Kearney, 2004). The UI for typical a-Si (300-780 nm) and c-Si (300-1050 nm) (Emery K. , 1986) modules is shown in Figure 2 for the same spectrum as in section 2.1.

[6] External quantum efficiency is similar to the internal quantum efficiency, but also accounts for reflection and absorption at the air-glass-module interface.

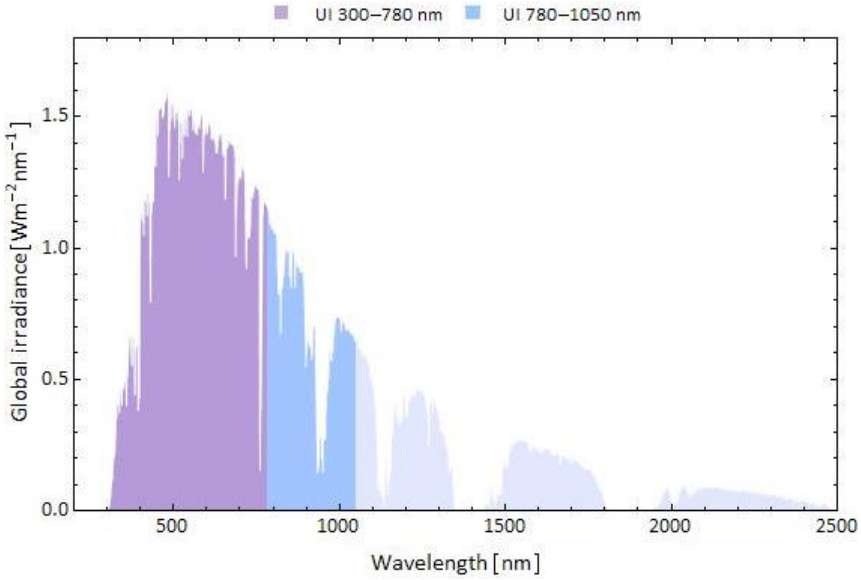

Figure 2 Air mass 1.5 standard spectrum ASTM G-173 (Emery K. , 2012) with a total irradiance of 1000 W/m^2. In purple, (300-780 nm) is the useful irradiance typically used for a-Si modules, $UI_{a\text{-}Si}$ =567 W/m^2. C-Si modules are sensitive to light with wavelength between 300-1050 nm (blue and purple area), resulting in a $UI_{c\text{-}Si}$ =775 W/m^2 (Emery K. , 1986). The corresponding average photon energy (300-1050 nm) is 1.89 eV.

2.3. AVERAGE PHOTON ENERGY

The useful irradiance is a module-specific characterization of the spectral irradiance and is unable to parameterize the irradiance without application to a specific module. More conveniently, a general characterization parameter is defined, such as given by the average photon energy (APE), defined as:

$$APE = \frac{\int_a^b E(\lambda)d\lambda}{q\int_a^b \Phi(\lambda)d\lambda} \qquad [1]$$

(Williams, Betts, Helf, Gottschalg, Beyer, & Infield, 2003) (Minemoto, et al., 2007). Here, q is the electron charge ($1.60217646 \cdot 10^{-19}$ C) and a and b are arbitrary wavelengths. Inter-comparison of APE values is possible only over an equal range of a and b. Finally, $\Phi(\lambda)$ is the photon flux density or the number of photons per wavelength interval, defined as: $\Phi(\lambda) = \frac{E(\lambda)}{h\,c/\lambda}$, where h is Planck's constant ($6.626068 \cdot 10^{-34}$ m^{2}kg/s) and c the speed of light (299792458 m/s). For equal total irradiance, a higher APE indicates a bluer spectrum, i.e. on average higher energy photons; a lower APE indicates a red-rich spectrum. Especially for low irradiance values that can result from various spectra, the APE allows to distinguish between them. Note that the average photon energy by itself does not contain information on the total energy content of the irradiance. The total irradiance therefore remains a key parameter.

3. PV PERFORMANCE

3.1. RATING: STANDARD TEST CONDITIONS

As mentioned before, PV performance is influenced by three environmental parameters. Since solar panels operate under a wide range of environmental conditions, performance rating as a function of these conditions is a laborious task. As a performance benchmark, solar panels are therefore rated under standardized conditions: standard test conditions (STC) developed by the American Society for Testing and Materials (ASTM). Standard test conditions comprise module temperature $T_{STC} = 25\,°C$, total irradiance $G_{STC} = 1000\,W/m^2$ and the ASTM G-173 standard spectrum, which is shown in Figure 2. Parameters that characterize the performance of a PV module, which are most commonly available on manufacturers' datasheets, are given in Table 1. Symbols are indicated that will be used throughout this report.

Table 1 Module specific parameters under standard test conditions commonly available on manufacturer's datasheets.

Parameter	Symbol	Unit
Short circuit current	I_{sc}	A
Open circuit voltage	V_{oc}	V
Current at mpp[7]	I_{mpp}	A
Voltage at mpp	V_{mpp}	V
Power at mpp	P_{mpp}	W
Number of cells	N_s	-
Short circuit current TC[8]	K_i	A/K
Open circuit voltage TC	K_v	V/K
Maximum power point TC	K_p	W/K

3.2. CHARACTERIZATION

The three most important performance indicators indicated in Table 1 are the short circuit current (I_{sc}), open circuit voltage (V_{oc}) and the power at the maximum power point (P_{mpp}). At zero bias voltage recombination and generation current eliminate one another so that $I_{sc} = I_{V=0}$ equals the photo current, I_{pv}, which is the current that is induced in the panel when exposed to solar irradiance. The short circuit current, however, does not contain direct information on the power that can be extracted from the cell as for this a potential difference is required. This is achieved by increasing the bias voltage, which has a maximum at V_{oc}. Increased voltage subsequently enhances dissipation currents within the cell, lowering the current that is available for power generation $I_{V>0} < I_{pv}$. The maximum power point provides the most optimal tradeoff between current and bias voltage in the solar cell, delivering $P_{mpp} = I_{mpp} \cdot V_{mpp}$. In appendix I, current-voltage (I-V) and power-voltage (P-V) characteristics under STC for different solar cells are shown.

Although P_{mpp} is the most useful parameter in PV performance modeling, it is strongly correlated with the short circuit current (Betts, 2004) (Beyer, Yordanov, Midtgard, Saetre, & Imenes, 2011). Determining I_{sc} is therefore of similar importance.

[7] Maximum power point

[8] Temperature coefficient, see next section.

3.3. MODELING

3.3.1. FIRST ORDER CORRECTIONS

In reality, standard test conditions hardly occur. For example, module temperatures rise above 25°C due to high incident irradiance. Temperature coefficients (TC) allow for correcting performance parameters for variations in module temperature. TCs indicate the increase in respective parameter per Kelvin of module temperature increase. A negative temperature coefficient indicates a decrease as temperature rises. The open circuit voltage and power corrected for variations in T yield:

$$V_{oc}(T, G_{STC}) = V_{oc(STC)} + K_v(T - T_{STC})$$

$$P_{mpp}(T, G_{STC}) = P_{mpp(STC)} + K_p(T - T_{STC}) .$$

Furthermore, for Isc/G constant, the short circuit current can be corrected for variations in G, by a first order relation (Betts, 2004):

$$I_{sc}(T, G) = [\, I_{sc(STC)} + K_i(T - T_{STC}) \,] \frac{G}{G_{STC}}, \qquad [2]$$

3.3.2. SPECTRAL RESPONSE

Outdoor conditions are, aside from STC temperature and total irradiance, rarely characterized by the ASTM G-173 standard spectrum, as the incident spectrum changes on an hourly basis, due to clouds, and on a daily and monthly basis due to the sun's changing overhead position. PV performance is influenced by the spectral distribution and therefore corrections are required for spectral variations. Chapter 2.2 briefly discussed the external quantum efficiency of PV modules, which quantifies the photon absorption efficiency. Performance efficiency i.e. the energy needed to induce current in the cell, however, is not fully captured by the EQE. High energy photons, $E_\varphi > E_g$, that are not reflected are inefficiently absorbed and lose their excess energy, $E_\varphi - E_g$, by thermalization, i.e. heating of the module. These effects are captured in more detail by the spectral response, $SR(\lambda) = \frac{q\,\lambda}{h\,c} EQE(\lambda)$, where q is the electron charge ($1.60217646 \cdot 10^{-19}$ C). Examples of spectral response curves of amorphous and crystalline silicon are shown in Figure 3. The spectral response indicates the ratio of induced current to incident photon energy as a function of wavelength. From the SR, the short circuit current then yields:

$$I_{sc} = A_{active} \cdot \int SR(\lambda) E(\lambda) d\lambda \qquad [3]$$

(Betts, 2004), where A_{active} is the module area and $SR(\lambda)$ is the spectral response in A/W.

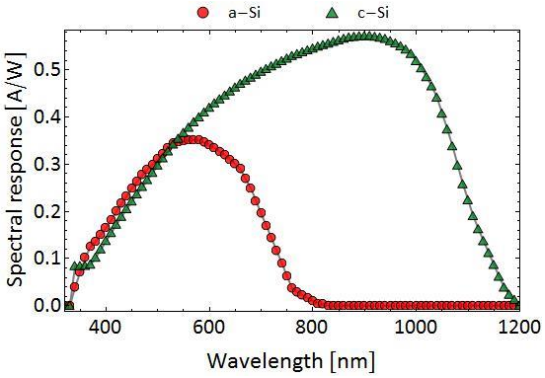

Figure 3 Typical spectral response for a-Si and c-Si modules, as a function of wavelength (Kate, 2012).

3.4. PV PERFORMANCE MODELING

3.4.1. MICROSCOPIC MODEL

Spectral effects can be easily accommodated in a PV performance model using equation 3. For this the spectral response is required, which is either to be measured, or calculated using a physical microscopic approach. The former requires specific equipment that allows for exposing the solar cell to irradiance in a small wavelength interval. Irrelevant for commercial applications, SR curves are therefore rarely supplied by the manufacturer. The latter requires detailed technical information on the cells, such as material dimensions, doping concentration, band gap etc. (Krishnan, et al., 2009). Since both SR-curves and specific technical data are not available, the seemingly simple equation 3 is unpractical. In this report, two macroscopic PV performance model approaches are used: A two-diode model, used as modeling benchmark, and an empirical model that corrects for spectral variations.

3.4.2. SIMPLE 2-DIODE MODEL

A PV module can be modeled as an electrical circuit containing one or several diodes (Twidell & Weir, 2006). A diode model's primary goal is reproducing the I-V characteristics of a solar cell under non-standard conditions. The equivalent circuit of a two-diode model is depicted in Figure 4. Here, I_{pv} is as before the photo or light induced current. I_{D1} and I_{D2} are the reverse saturation currents, I_o, of diode 1 and 2 respectively, anti-parallel to the light induced current. I_{D1} accommodates recombination losses due to the diffusion current as the bias voltage increases, as mentioned in section 3.2. The two-diode model is an extension to the single-diode model by inclusion of a second diode. This diode corrects for the recombination current (I_{o2}) in the junction which dominates at low forward-bias voltage (Chih-Tang, Noyce, & Shockley, 1957). R_s (R_{series}) and R_p (R_{shunt}) are the series and shunt resistances respectively, which are module specific parameters. R_s accounts for the internal electrical resistance of the cell, such as resistance at the contacts; R_p accounts for design flaws in the cell which provide an alternative path parallel to the external load. Good solar cells therefore have low R_s and high R_p (Twidell & Weir, 2006). The two-diode model equation is given by:

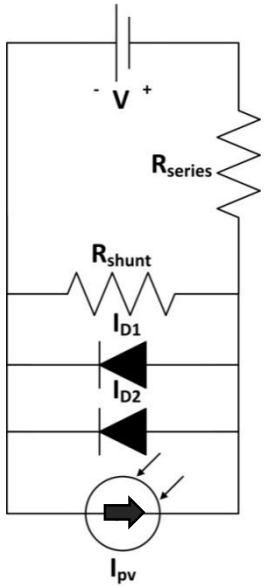

Figure 4 Equivalent electric circuit of a two-diode PV model.

$$I = I_{PV} - I_{o1}\left(exp\left[\frac{V+IR_s}{a_1 V_T}\right] - 1\right) + I_{o2}\left(exp\left[\frac{V+IR_s}{a_2 V_T}\right] - 1\right) - \left(\frac{V+IR_s}{R_p}\right) \quad [4]$$

(Chih-Tang, Noyce, & Shockley, 1957), where $V_T = N_s k\, T/q$ is the thermal voltage. Equation 4 requires computation of 7 parameters: I_{o1}, I_{o2}, a_1, a_2, I_{pv}, R_s, and R_p. a_1 and a_2 are the ideality factors of diode 1 and 2, which are unity if the diode behaves perfectly and close to two for non-ideal behavior. The iteration processes involved to compute these parameters, from rated performance under STC, are time consuming and are therefore not convenient for fast data processing (Ishaque, Salam, & Taheri, 2011). The simple two-diode model proposed by (Ishaque, Salam, & Taheri, 2011) that is presented here simplifies these calculations by using analytical expressions for 5 out of the 7 parameters, reducing equation 4 to equation 5. $I_{pv}(\approx I_{sc})$ is calculated using equation 2 and I_{o1} and I_{o2} are calculated using equation 7. The ideality factors, a_1 and a_2, are set to 1 and 1.2 respectively as these values yield the best agreement between model and measurements (Ishaque, Salam, & Syafaruddin, 2011).

$$I = I_{PV} - I_o\left(exp\left[\frac{V+IR_S}{a_1 V_T}\right] + exp\left[\frac{V+IR_S}{a_2 V_T}\right] - 2\right) - \left(\frac{V+IR_S}{R_p}\right) \quad [5]$$

The two remaining parameters, the shunt and series resistances, are calculated using iteration: R_s is stepwise increased while R_p is calculated using equation 6. For each R_s-R_p-pair the I-V characteristics are calculated by numerically solving equation 5 using the Newton-Raphson method[9]. From the current-voltage characteristics the maximum power points is determined and compared to the tabulated rated power ($P_{mpp(STC)}$). If the difference between modeled and tabulated values is more than tolerated, the process is repeated for slightly increased R_s.

$$R_p = \frac{V+IR_S}{I_{PV} - I_o\left(exp\left[\frac{V+IR_S}{a_1 V_T}\right] + exp\left[\frac{V+IR_S}{a_2 V_T}\right] - 2\right) - \left(\frac{V+IR_S}{R_p}\right) - I}_{I \,\&\, V\ @MPP} \quad [6]$$

$$I_{o1} = I_{o2} = I_o = \frac{I_{sc(STC)} + K_i \Delta T}{exp\left[\frac{V_{oc(STC)} + K_v \Delta T}{V_T}\right] - 1} \quad [7]$$

The simple two-diode model (equation 5) allows for more accurate results than a single-diode model and faster computational time than a regular two-diode model (equation 4) (Ishaque, Salam, & Syafaruddin, 2011). Inputs are module temperature, total integrated irradiance and module parameters at STC that are commonly available on manufacturers' datasheets (see Table 1). Having determined R_s and R_p under STC in step 1, the I-V and P-V curves for arbitrary module temperature and irradiance can be computed in step 2. The algorithm that is used in this model is shown in Figure 5.

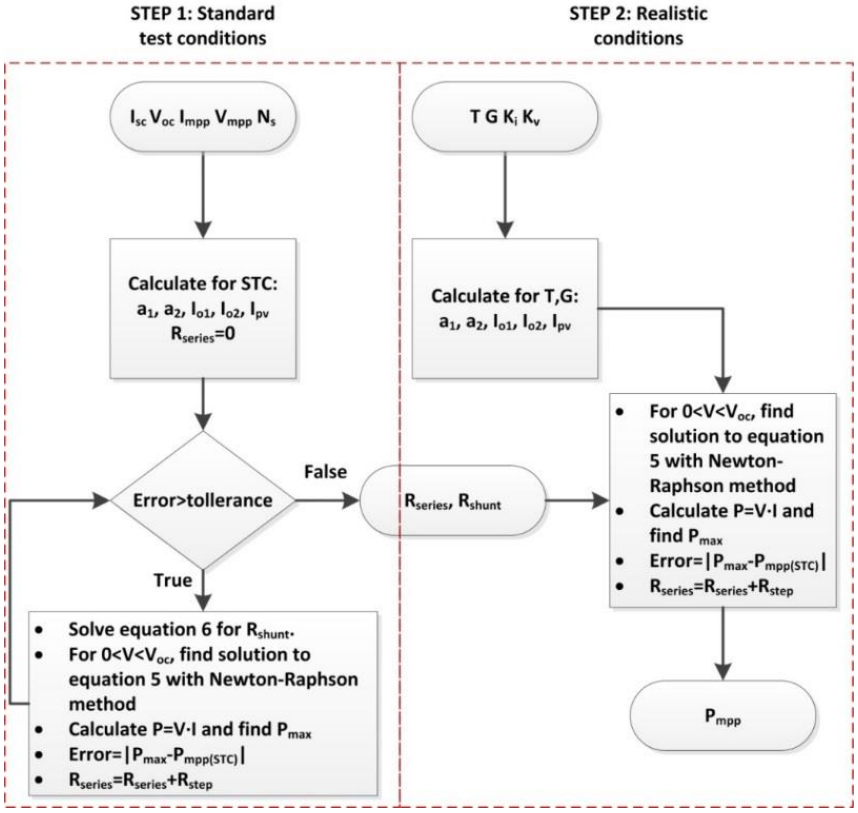

Figure 5 Schematic representation of the two-diode model. The left hand side illustrates the algorithm used to calculate the series and shunt resistance. The right hand side simulates the performance under realistic conditions. Rounded boxes represent inputs and outputs (Ishaque, Salam, & Syafaruddin, 2011).

[9] As a built-in function of Wolfram Mathematic 8, the Newton-Raphson method numerically approximates the roots of x for which f(x)=0, by means of derivatives. The method has quasi-quadratic convergence around the roots.

3.4.3. EMPIRICAL MODEL

3.4.3.1. MODELING THE SHORT CIRCUIT CURRENT

An empirical model for I_{sc} and P_{mpp} is presented in (Beyer, Gottschalg, Betts, & Infield, 2003), (Beyer, Yordanov, Midtgard, Saetre, & Imenes, 2011) and (Betts, 2004). The model is based on empirical expressions for I_{sc} and P_{mpp}, which require the computation of multiple fitting constants. This model therefore requires additional data to the STC reported on the manufacturer's datasheets. Once computed for a specific panel however, the model can simulate outdoor performance. The short circuit current response I_{sc}/G is modeled by:

$$\frac{I_{sc}(T,G)}{G} = (c_0 + c_1 T)\,, \qquad [8]$$

where c_0 and c_1 are device specific parameters. This expression can be solved analytically for c_0 and c_1 from data that is available on the datasheets. Reminding that the short circuit current I_{sc} and $I_{sc(STC)}$ are related by the temperature coefficient, K_i, it is easily shown that $c_0 = (\frac{I_{sc(STC)}}{G_{STC}} - c_1 T_{STC})$ and $c_1 = \frac{K_i}{G_{STC}}$, so that equation 8 is equivalent to equation 2.

Equation 8 does not capture spectral effects due to the nature of G. This poses a problem for amorphous-silicon modules. The short circuit current can be improved by replacing G by the useful fraction UI (Beyer, Gottschalg, Betts, & Infield, 2003):

$$I_{sc} = \left(I_{sc,STC} + K_i(T - T_{STC})\right)\frac{UI}{UI_{STC}}. \qquad [9]$$

Here, UI_{STC} is the useful irradiance of the ASTM G-173 standard spectrum. Note that UI and therefore UI_{STC} are device specific parameters that depend on the type of the semiconductor material.

In order to accommodate spectral effects in more detail, (Betts, 2004) suggests an empirical relation between the normalized, temperature corrected, current response and APE. This relation yields a third order polynomial, where the parameters b_i are obtained through least squares fitting:

$$\frac{I_{sc}/G - K_i/G_{STC}(T - T_{STC})}{I_{sc,STC}/G_{STC}} = b_1 + b_2 APE + b_3 APE^2 + b_4 APE^3. \qquad [10]$$

3.4.3.2. MODELING THE POWER AT THE MAXIMUM POWER POINT.

This empirical model has no electrical analogies, but approximates the P_{mpp} by least squares fitting (Beyer, Yordanov, Midtgard, Saetre, & Imenes, 2011). The power response of the PV module is given by:

$$\frac{P_{mpp}}{I_{sc}} = \left(a_1 + a_2 I_{sc} + a_3\, ln(I_{sc}/I_{sc0})\right)[1 + a_4(T - T_{STC})]. \qquad [11]$$

Here a_1, a_2, a_3 and a_4 are device specific parameters that are either to be measured or obtained from appropriate datasheets[10]. Note that a_4 equals the normalized P_{mpp} temperature coefficient, $\frac{K_p}{P_{mpp(STC)}}$. I_{sc0} is an arbitrary number with unit Ampère to make the argument of the logarithm dimensionless, e.g. $I_{sc0} = 1\ A$. I_{sc0}, however, must be used consistently, as the constant a_3 is dependent on it.

[10] Note that at least four $P_{mpp}(I_{sc})$ data points are needed in order to analytically solve this equation for the four fitting constants. Since datasheets commonly only supply STC, this model has to be calibrated under outdoor conditions first.

4. VALIDATION

4.1. EXPERIMENTAL SETUP

Permission was granted by EKO Instruments Europe to use experimental data from a test setup in The Hague (52.063586° latitude, 4.316972° longitude) for model validation. The experimental setup consists of four types of panels facing south on a 35° tilt, among which crystalline- and amorphous-silicon modules. Specifications from respective manufacturer's datasheets are shown in Table 2. Furthermore, a pyranometer, a sensor for temperature measurements on the backside of the panels and a spectroradiometer are installed, which allows one to study Dutch environmental conditions and moreover to study spectral effects. Data is available from June 16 2012, as this was the day the first set of reliable data that was acquired. Part of the experimental setup is shown in Figure 6.

Table 2 Specifications, as supplied by the manufacturer, of the four PV modules that are tested in the EKO Instruments Europe test facility.

Brand	Name	Type	N_s	P_{mpp}	V_{mpp}	I_{mpp}	I_{sc}	V_{oc}	K_i	K_v	K_p
				W	V	A	A	V	%/K	%/K	%/K
Solon	Black 230/07	Mono c-Si	60	235	29.4	8.0	8.75	36.5	0.03	-0.33	-0.43
BP	3230N	Poly c-Si	60	230	29.2	7.9	8.7	36.4	0.065	-0.36	-0.5
Gadir	a-SiT Translucent	Thin film a-Si	80	95	105	0.9	1.14	138	0.04	-0.28	-0.21
Flexcell	MO75	Thin film a-Si	- [11]	85	55	1.5	2.0	68	0.086	-0.237	-0.15

Figure 6 Picture of the test installation of EKO Instruments Europe, showing two crystalline solar panels on the left and the equipment to measure incident spectral irradiance on the right. The amorphous-silicon modules are not captured in this picture, but are located to the right side (source: EKO Instruments Europe).

[11] Unknown, not available from datasheet.

4.1.1. PV PANEL PERFORMANCE

Every 5 minutes the I-V curve is measured using a MP-160 I-V curve tracer and performance parameters I_{sc}, V_{oc}, P_{mpp}, I_{mpp}, and V_{mpp} are calculated. This measurement is accompanied by the module temperature and total irradiance at the start of the measurement. It is important that during the I-V curve measurement, environmental conditions remain equal to the initial conditions so that the resulting I-V curve represents PV performance under these conditions. If environmental conditions vary during the measurement, e.g. due to a transit cloud, a composition of different IV-curves results. The MP-160's fast measuring time of a few milliseconds, however, ensures that irradiance variations are no issue (Los, 2012)

4.1.2. PYRANOMETER

Using a MS-802 pyranometer the total global irradiation, direct and diffuse, is measured on a 35° tilted surface. To reduce shading by the pyranometer on the PV panels, it is installed aside the PV panels as shown in Figure 6. Global irradiation measurements by the pyranometer can therefore be used to approximate the global irradiance on the PV panels, if light shines homogeneously on both the panels and the pyranometer. If clouds do not cause sharp shading patterns and there are no objects around that can obscure either the panel or the pyranometer, this assumption holds.

4.1.3. SPECTRORADIOMETER

The spectrum of the incident solar irradiation was acquired every minute with a MS-700 spectroradiometer, covering a wavelength range of 350 to 1050 nm. PV modules are usually spectrally responsive within this interval (see Figure 3) and therefore this range is sufficient to study spectral effects on PV performance. Consequently, 350 to 1050 nm is taken as range for calculation of the average photon energy (equation 1) throughout this report. The range of the useful irradiance as given in chapter 2.2, however, cannot fully be used as the lower limit lies outside the detection range of the spectroradiometer. Hence, UI limits are adjusted to 350-780 nm and 350-1050 nm for a-Si and c-Si respectively. As an indication, for the ASTM G-173 spectrum, this adjustment reduces the UI for c-Si and a-Si by 1.8 % and 2.4 % respectively. Since the spectral response is low between 300 and 350 nm this is anticipated to have little effect.

4.2. DATA SELECTION

Output data and spectral irradiance parameters, G, UI and APE, were joined by matching both the date and time label. This resulted in PV performance and spectral data with a 5 minute interval. Measurements with low irradiance, i.e. $G < 10\ W/m^2$, were rejected due to poor signal-noise ratio. Model validation is carried out for four clear days (23-26 July 2012). Clear days were chosen for analysis for two reasons:

Firstly, clouded days exhibit performance data points with large deviation from the general trend. These extreme values are unrealistic and are most likely caused by measuring defects. These extremes can manually be excluded from analysis. Nevertheless, there are possibly shading effects that cause additional data errors, which do not deviate significantly from the general trend. It is much harder to trace and excluded these errors. Clear days do not display shading effects due to absence of clouds and therefore studying clear days will ensure less systematical measuring errors. Secondly, spectral irradiance varies more smoothly on clear days compared to clouded days, as shown in Figure 8. Changes in environmental conditions on clear days are therefore easier understood and studied as there is no abrupt disturbance by clouds. When outdoor performance variations on ideal, clear days are understood, the study could be extended to clouded days. In the final chapter of this report, there will be a few words on extending the framework of this research to clouded days.

4.3. DEFINITIONS

4.3.1. MODELING ACCURACY

Different definitions exist to quantify the modeling error, among which mean bias error (MBE), mean absolute error (MAE) and root mean squared error (RMSE):

$$MBE = \frac{1}{n}\sum_{i=1}^{n} e_i$$

$$MAE = \frac{1}{n}\sum_{i=1}^{n} |e_i|$$

$$RMSE = \sqrt{\frac{1}{n}\sum_{i=1}^{n} {e_i}^2}.$$

Here, $e_i = (x_{mod,i} - x_{exp,i})$ equals the residual value between modeled, $x_{mod,i}$, and measured value ,$x_{exp,i}$, with n the number of data points. MBE equals the mean of the residuals and indicates if the model, on average, tends to overestimate ($MBE > 0$) or underestimate ($MBE < 0$) the experimental data. The MAE and RMSE quantify the average modeling accuracy (Willmott & Matsuura, 2005).

RMSE depends on the mean residual value, on the variability of the residuals and the sample size, n. As a result the RMSE is more sensitive to large residual value and is always $\geq MAE$ for an identical dataset. The mean absolute error is unambiguously defined and is therefore preferred above RMSE for determining the accuracy (Willmott & Matsuura, 2005). MAE is therefore used to quantify the modeling accuracy in this report. Nonetheless, the RMSE is given for comparison with literature where the RMSE is commonly used.

Inter-comparison of different models requires dimensionless quantities, which are obtained by dividing the MBE, MAE and RMSE by the measured mean value: $\overline{x_{exp}} = \frac{1}{n}\sum_{i=1}^{n}(x_{exp,i})$ (Demain, Journée, & Bertrand, 2012).

4.3.2. MODEL ANALYSIS

Both the relative modeling error in P_{mpp}, $\frac{P_{mod,i}-P_{exp,i}}{P_{exp,i}}$, and the quantitative error as described above are calculated for each module. However, the average modeling accuracy over the entire irradiance range is not indicative of where the model fails to simulate performance under realistic conditions. Therefore the total irradiance was divided into 50 W/m^2 intervals over which the analysis was carried out. These intervals do not necessarily contain an equal amount of data points, which is good example of why the MAE is preferred above the RMSE.

4.3.3. SPECTRAL CHARACTERIZATION UNDER STANDARD TEST CONDITIONS

Modeling the performance of PV modules under realistic conditions, involves corrections of PV performance parameters under STC, such as presented in chapter 3.4.3. Inclusion of spectral information in the empirical models requires calculation of the spectral parameters of the ASTM G-173 standard spectrum. For the limits of the useful fraction and average photon energy given in section 2.2, conditions under STC are given in Table 3.

Table 3 Environmental parameters as defined by STC, but limited by the experimental setup.

Parameter	Symbol	Value	
Module temperature	T_{STC}	25	°C
Total irradiance	G_{STC}	1.000	kW/m^2
Useful irradiancea-Si[12]	$UI_{a\text{-}Si(STC)}$	0.553	kW/m^2
Useful irradiance c-Si[13]	$UI_{c\text{-}Si(STC)}$	0.761	kW/m^2
APE[13]	APE_{STC}	1.88	eV

[12] 350-780 nm
[13] 350-1050 nm

5. DATA DISTRIBUTION

5.1. PV PERFORMANCE

A plot of the power versus irradiance (Figure 7) on clear days, shows that on moments with equal total irradiance, in particular c-Si modules perform better in the afternoon than in the morning[14]. This is counter-intuitive since the module remains the same device during the day. The deviation in morning and afternoon must therefore be caused by different environmental conditions, which are clearly not revealed by changes in the total irradiance. During the day, module temperature has risen due to heating by solar irradiation. Performance, however, is expected to decrease as temperature rises, represented by a negative P_{mpp} temperature coefficient (Table 2). Based on temperature, modules are therefore expected to perform better in the morning than in the afternoon, displaying the reverse effect of that seen in Figure 7. Chapter 2 briefly discussed the inability of the total irradiance to capture spectral information. As total irradiance and temperature have been accounted for, there must be a change in spectral distribution that causes the difference between morning and afternoon. This is further examined in the next section.

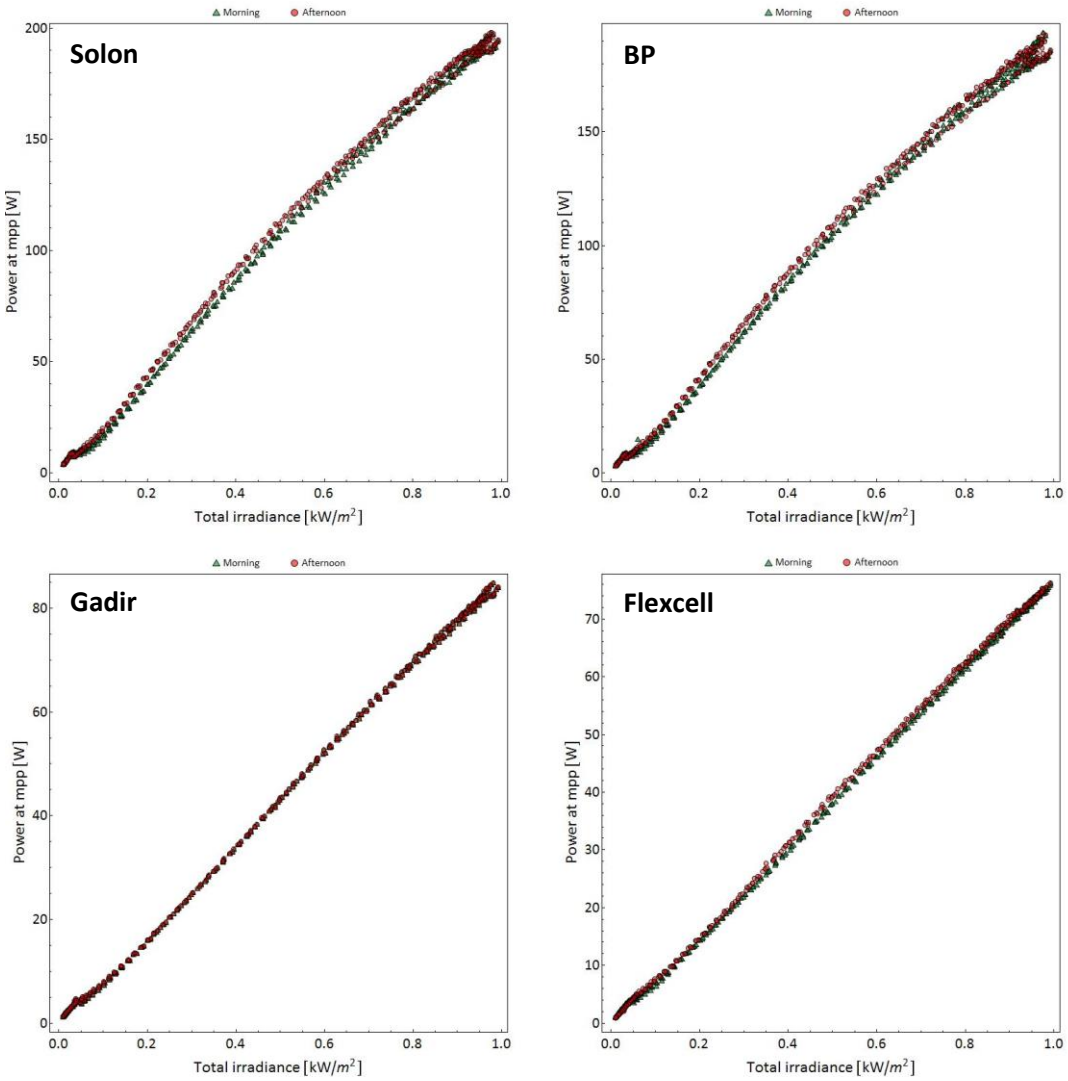

Figure 7 Measured power at the maximum power point versus total irradiance for the morning and afternoon on four clear days (23-26 July 2012).

[14] Morning represents the day from sunrise to noon; afternoon represents the day from noon to sunset.

5.2. ENVIRONMENTAL CONDITIONS

Figure 8 shows that a clear day is characterized by smooth variations in total and useful irradiance as a result of the sun's changing overhead position. Naturally, the useful irradiance is lower than the total irradiance, but follows a similar distribution, which appears to be symmetrical around solar noon. A clouded day is shown for reference at the bottom of Figure 8, which exhibits abrupt variations in irradiance due to transit clouds.

Observing the average photon energy learns that clouded days exhibit a bluer spectrum than clear days. This is caused by light scattering by clouds which enhances short wavelength diffuse irradiation (Betts, 2004). On clear days, the APE remains approximately constant during the day, with a slight red-shift around 7-8 hour and 16-17 hours. The red-shift originates from the high air mass (high solar zenith angle) in the morning and evening, which enhances scattering of mainly short wavelength photons (Betts, 2004). Hence, the contribution of blue light to the direct irradiance decreases and shifts towards diffuse irradiance. Overall, the contribution of short wavelength light to the total irradiance is reduced and consequently the incident spectrum is red-shifted.

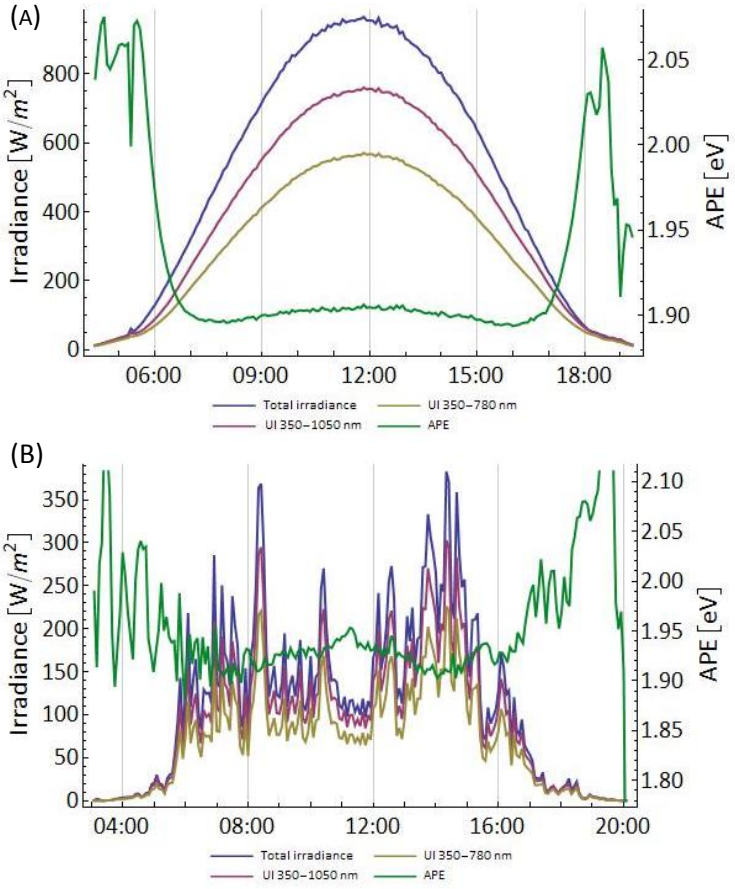

Figure 8 Spectral irradiance variations on a clear (A, July 23, 2012) and clouded day (B, July 18, 2012).

Early in the morning and late in the evening, however, when the sun is in the east and west respectively, the APE shows rapid increase. Since here the sun is situated behind the module plane (Betts, 2004), this low irradiance is exclusively diffuse. As a result of the high air mass, the diffuse irradiance is blue shifted and is characterized by a higher APE. The slight kink in the total irradiance curve at approximately 5:30 indicates the moment when the array is also exposed to direct irradiance; around 18:00 the opposite is true.

From Figure 8A it is, however, not apparent if the spectrum in the afternoon differs from that in the morning. Spectral variations on clear days are closer examined in Figure 9, which shows the variation of the spectral characterization parameters discussed in chapter 2 versus the total irradiance. From the two trends observed in the useful irradiance, it follows that the spectral irradiance is asymmetrical around solar noon and is in fact lower in the morning than in the afternoon. Since spectral irradiance is determined by interactions of the light in its path towards to observer, it can be deduced that this path is different in the morning and afternoon. As it concerns clear days only a difference in atmospheric composition must be the cause of the different incident spectra; apparently, light in the morning, shining from the east, encounters different atmospheric conditions than in the afternoon, where light shines from the west.

Furthermore, the APE is approximately constant for high incident irradiance, i.e. $APE_{\mathrm{G>0.2\ kW/m^2}} \approx 1.90\ \mathrm{eV}$, whereas low irradiance is characterized by higher APE. For $G < 0.05\ kW/m^2$ the sun in situated behind the panel and hence the irradiance is exclusively diffuse.

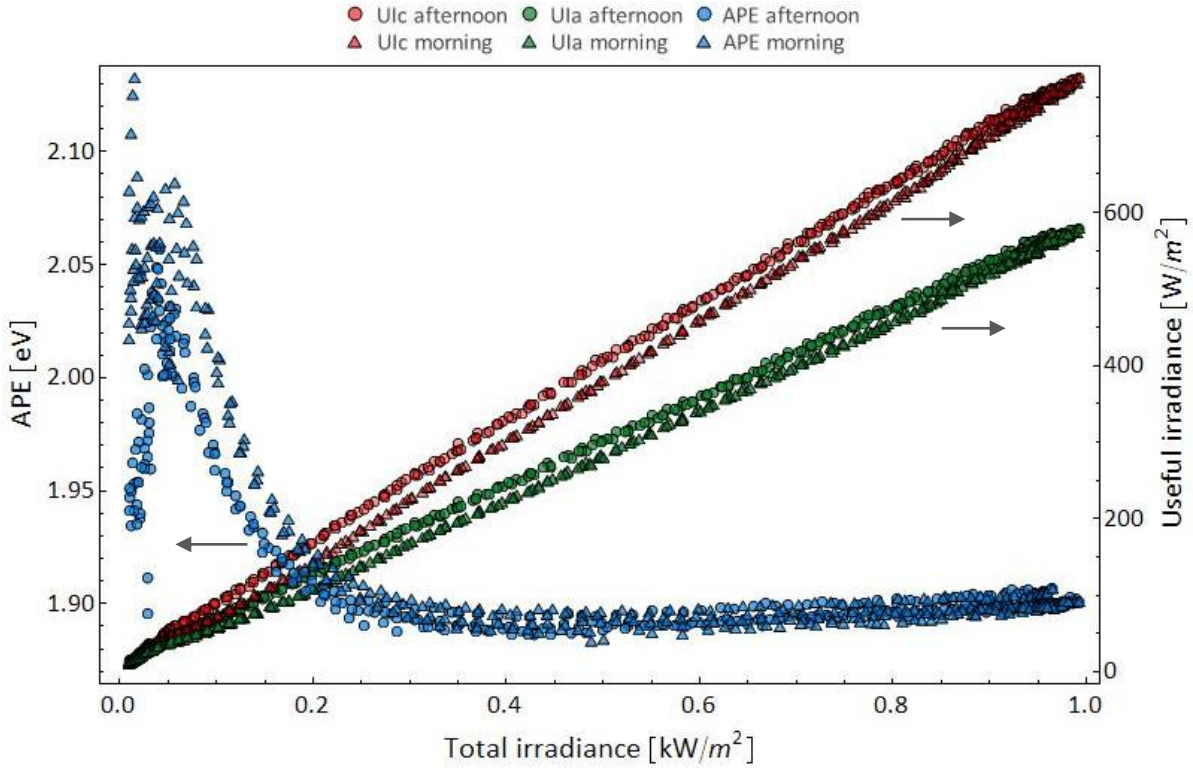

Figure 9 Useful irradiance (right axis) for c-Si (red) and a-Si (green) and average photon energy (blue, left axis) versus total irradiance on four clear days (23-26 July 2012).

5.3. CONCLUSIONS

The P_{mpp} on clear days displays a discrepancy between morning and afternoon. Since the modules themselves remain unchanged, the discrepancy must be a result of a change in spectral distribution. Among the characterization methods examined, especially the useful irradiance exhibits similar discrepancy, which supports this hypothesis. The APE additionally reveals a blue-shift of the spectrum at low incident irradiance. Both observations qualitatively indicate that the total irradiance by itself is not sufficient for characterization of the incident irradiance and subsequently for accurate performance modeling, as the spectral distribution of the irradiance varies throughout the day.

6. MODELING RESULTS

6.1. SIMPLE TWO-DIODE MODEL

Performance is calculated using the simple two-diode model presented in chapter 3.4.2. The calculated values of the shunt and series resistance are given in Appendix I. The number of cells per module for the Flexcell solar panel is unknown and because this is a required input of the two-diode model, this module is excluded from analysis. Any PV performance model should be accurate without discriminating between morning and afternoon and therefore analysis is performed for the entire four clear days. Nonetheless a graphical distinction was made between morning and afternoon, in order to monitor the discrepancy presented in section 5. Furthermore, the MAE was calculated over 50 W/m^2 irradiance intervals, represented by a horizontal line connecting two symbols.

6.1.1. SOLON

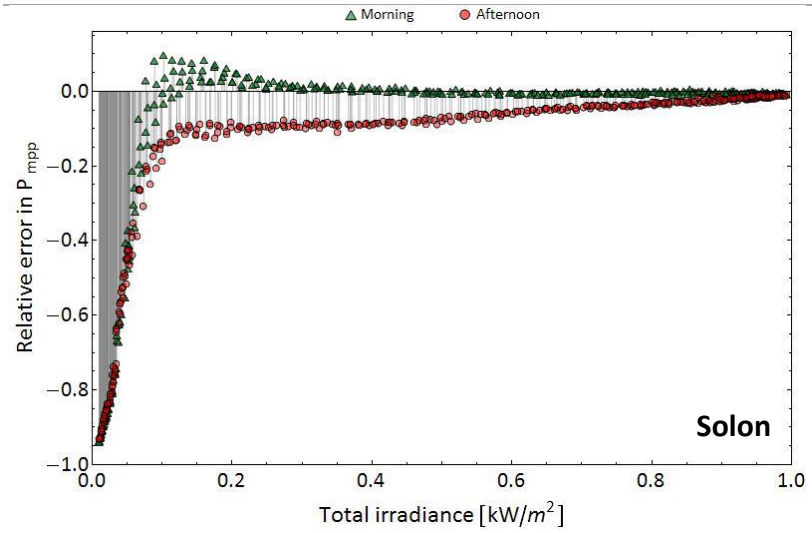

Figure 10 Relative modeling error in P_{mpp} for the Solon module on clear days in July.

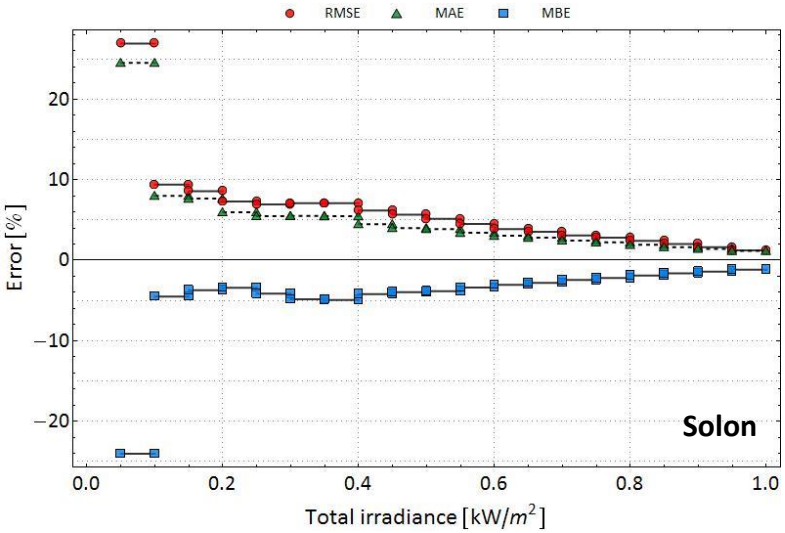

Figure 11 Modeling error in P_{mpp} for the Solon module on clear days in July on 50 W/m^2 intervals in total irradiance.

6.1.2. BP

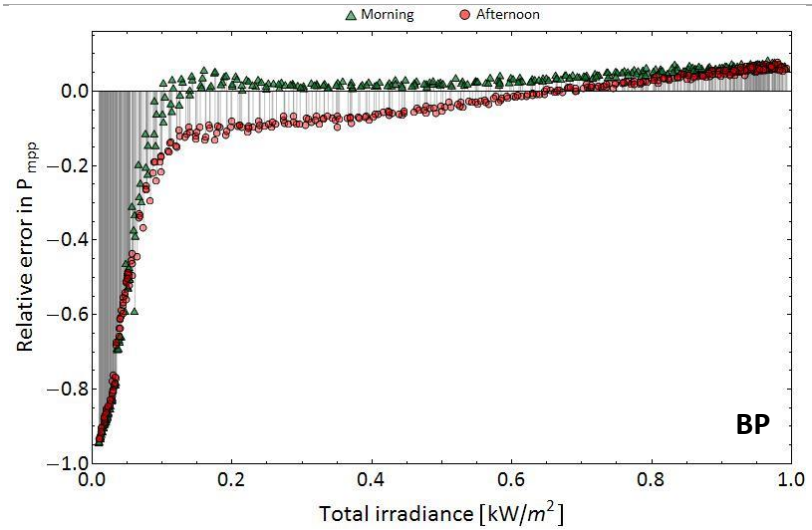

Figure 12 Relative modeling error in P_{mpp} for the BP module on clear days in July.

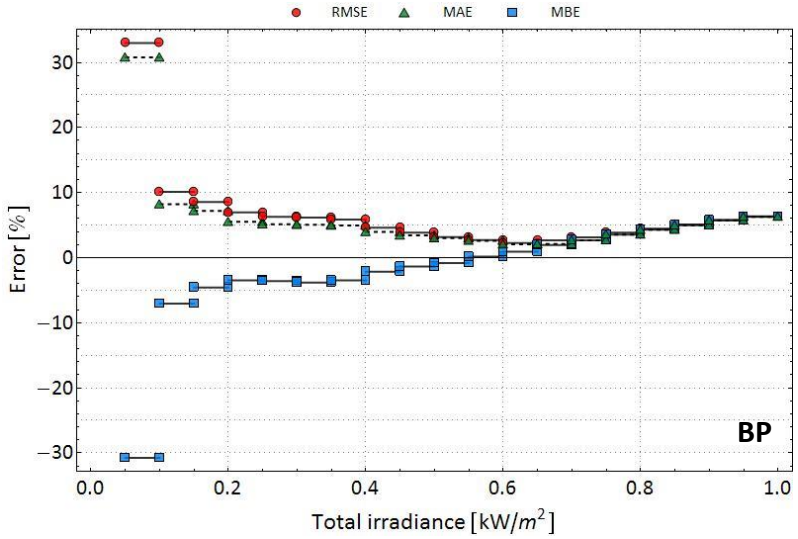

Figure 13 Modeling error in P_{mpp} for the BP module on clear days in July on 50 W/m² intervals in total irradiance.

6.1.3. GADIR

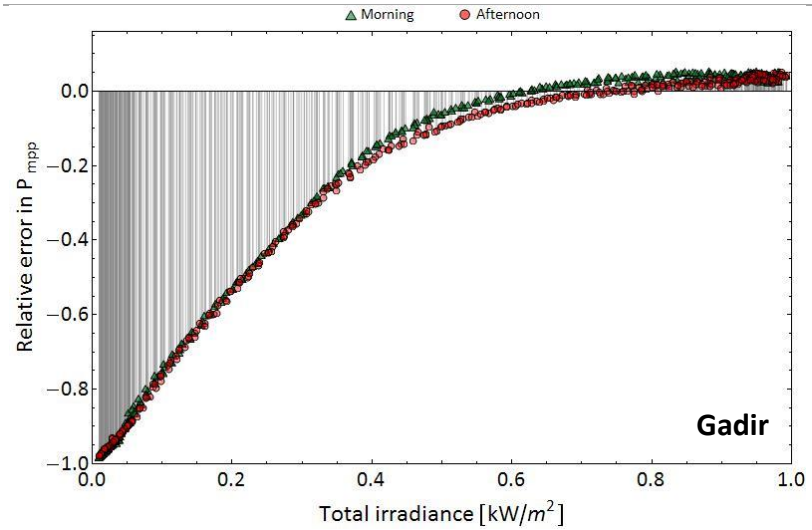

Figure 14 Relative modeling error in P_{mpp} for the Gadir module on clear days in July.

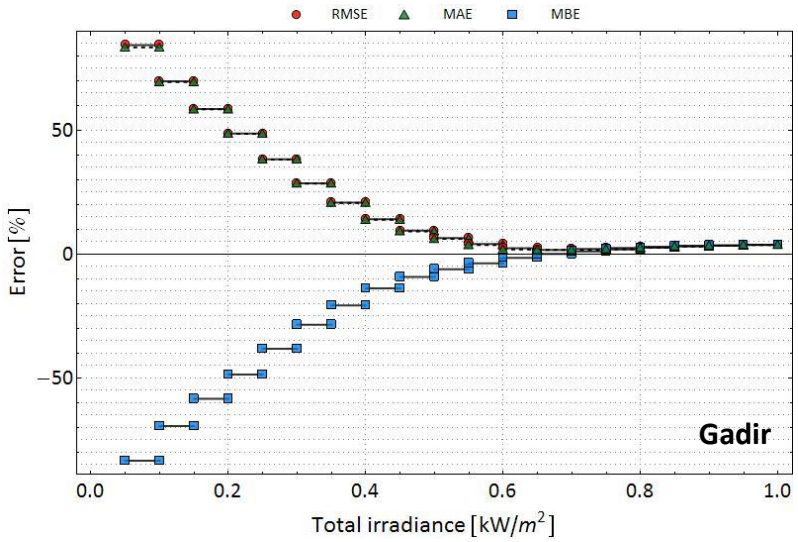

Figure 15 Modeling error in P_{mpp} for the Gadir module on clear days in July on 50 W/m² intervals in total irradiance.

6.1.4. CONCLUSIONS

The two-diode model simulates the outdoor performance of both crystalline PV panels with a MAE of below $\sim 5\%$. Inputs to this model, T and G, are unable to capture the change in spectral distribution and therefore the discrepancy between afternoon and morning is observed as discussed in chapter 4.2. The morning coincides best with measurements; the performance in the afternoon is underestimated, which originates from the relatively higher P_{mpp} in the afternoon (Figure 7). For low irradiance, $G < 0.1\ kW/m^2$ the modeling error increases significantly. Apparently, from this point down, the solar cell's behavior deviates from that of an ideal double-diode.

The amorphous-silicon Gadir solar panel greatly underestimates the outdoor performance up to $G = 0.6\ kW/m^2$. Only under high irradiance, $G > 0.6\ kW/m^2$ there is reasonable agreement ($MAE \approx 5\%$) between measurement and model.

The results presented above demonstrate that c-Si panels can be accurately described by a two-diode equivalent circuit. However, for $G < 100\ W/m^2$, the model breaks down. A-Si based modules can only be simulated by this equivalent electrical circuit under high irradiance and therefore require a different modeling approach.

6.2. EMPIRICAL MODEL

Three out of four fitting-parameters (equation 11) were obtained by least-squares fitting on the first clear day, July 23. The fourth parameter, a_4, was calculated via the P_{mpp} temperature coefficient as given in Table 2. Using these parameters P_{mpp} was then modeled for the four clear days, with G and T as input and with UI and T as input via equation 8 and 9 respectively. The fitting procedure is illustrated for the Solon module in Figure 16. A few data points at short circuit current close to one disagree with the fitted curve. Low short circuit current corresponds to low incident irradiance and these points might therefore be caused by poor signal-noise ratio. As it concerns only a few points, this is expected to have little effect on the fitted regression line.

The results for the modeled P_{mpp} are shown in the next sections; additionally in appendix II the fitting procedure for the remaining panels is presented, together with the RMSE and MBE of the modeled performance.

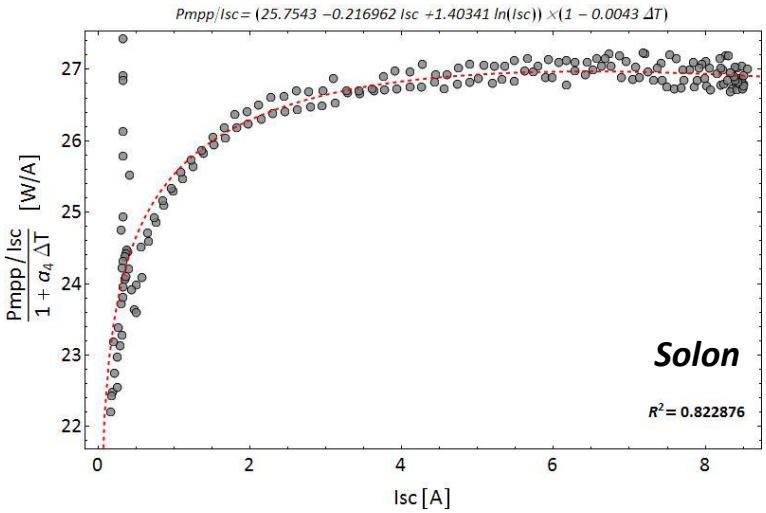

Figure 16 Power-current response least-squares fit (equation 11) on July 23 for the Solon module. The fitted equation is shown together with the coefficient of determination, R^2, (ranging from 0 to 1) that indicates how well the fit matches the data.

6.2.1. CRYSTALLINE-SILICON

6.2.1.1. SOLON MODULE

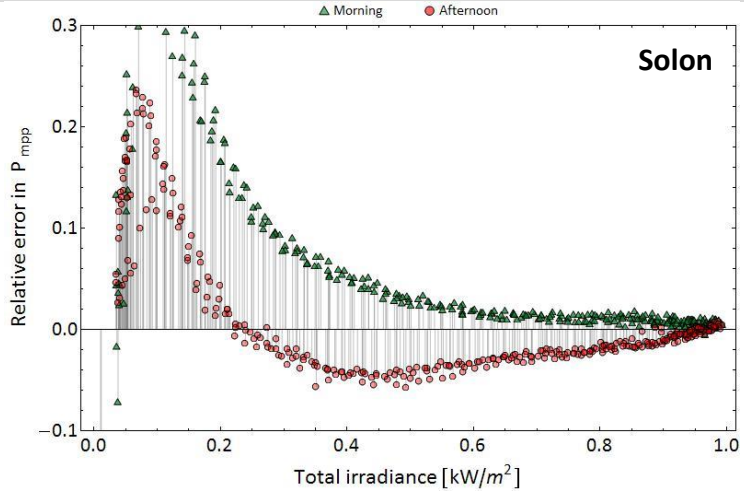

Figure 17 Relative modeling error in P_{mpp} for the Solon module, with total irradiance (G) and module temperature (T) as model inputs.

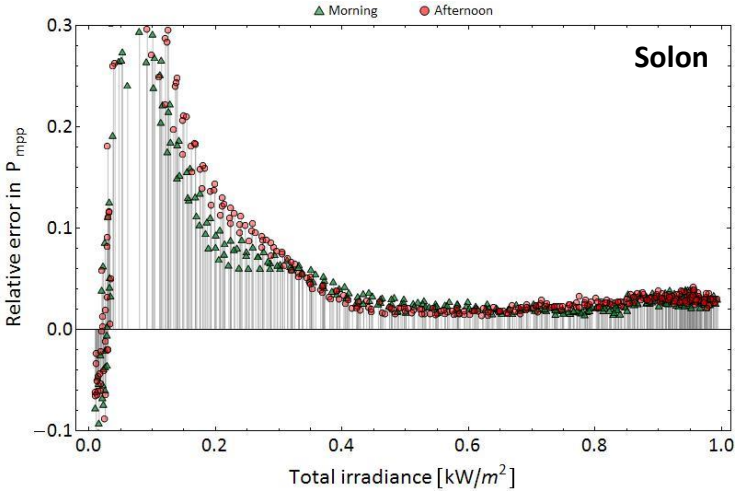

Figure 18 Relative modeling error in P_{mpp} for the Solon module, with useful irradiance (UI) and module temperature (T) as model inputs.

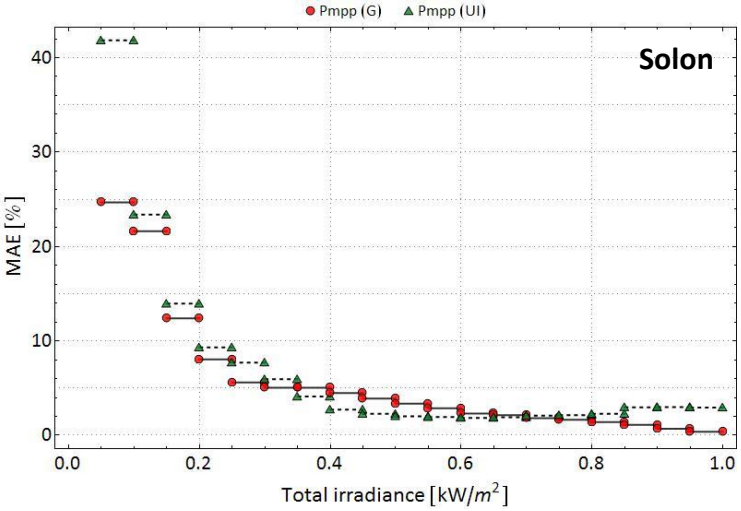

Figure 19 Mean absolute modeling error in P_{mpp} for the Solon module on clear days in July on a 50 W/m² irradiance interval.

6.2.1.2. BP MODULE

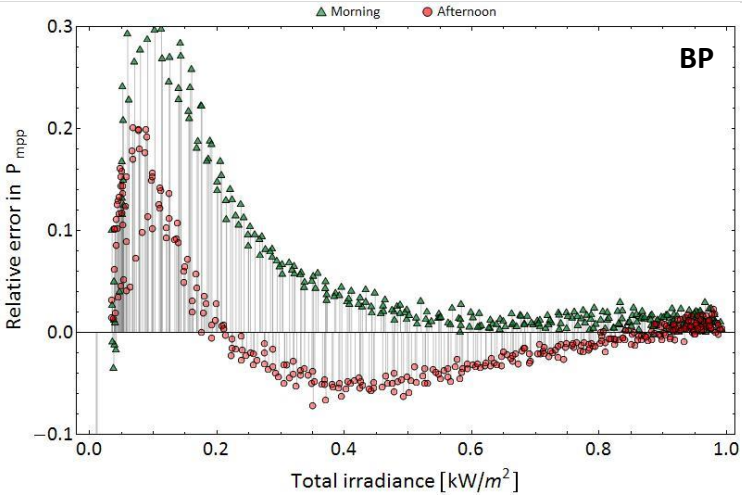

Figure 20 Relative modeling error in P_{mpp} for the BP module, with total irradiance (G) and module temperature (T) as model inputs.

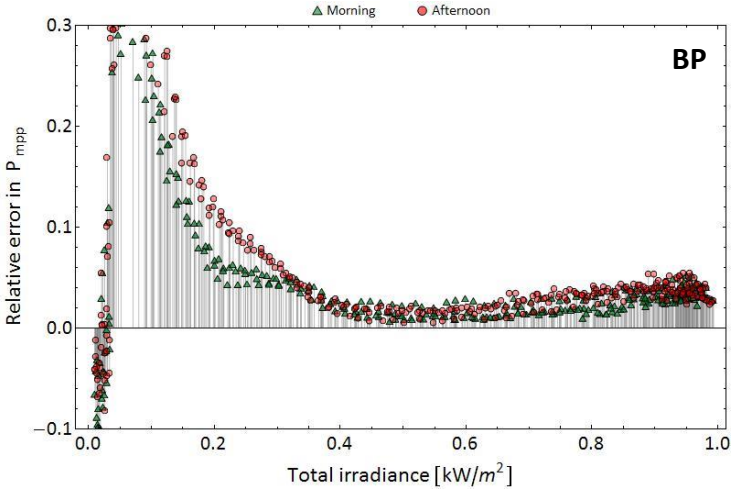

Figure 21 Relative modeling error in P_{mpp} for the BP module, with useful irradiance (UI) and module temperature (T) as model inputs.

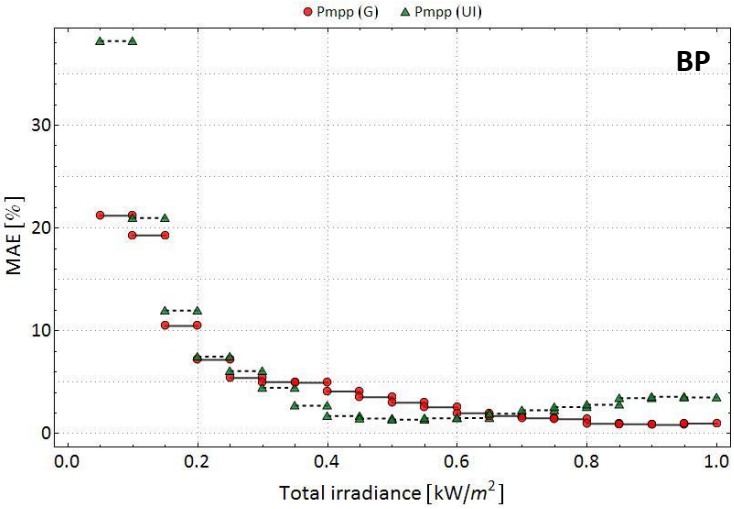

Figure 22 Mean absolute modeling error in P_{mpp} for the BP module on clear days in July on a 50 W/m² irradiance interval.

6.2.1.3. CONCLUSIONS

The solon and BP modules show similar results. In the afternoon, useful irradiance is higher than in the morning (see Figure 9), which leads to underestimation and overestimation by the empirical model respectively. For low irradiance values, $G < 0.3\ kW/m^2$, the model exhibits large deviation from outdoor measurements.

Accounting for spectral changes by replacing G by the useful fraction, results in less contrast between morning and afternoon (Figure 18 and Figure 21). However, the modeling accuracy at high irradiance is slightly reduced. Figure 19 and Figure 22 show the relative MAE for different irradiance intervals. MAE slightly improves by 1-2% points in the intermediate irradiance range, between $0.4 - 0.7\ kW/m^2$. Especially the afternoon is affected by accommodation of the UI, which is clear from Figure 18 and Figure 21. The spectral irradiance difference between morning and afternoon for this range is thus better captured by the UI than by G. However, the peak observed at low irradiance is not improved upon by inclusion of the useful irradiance.

6.2.2. AMORPHOUS-SILICON

6.2.2.1. GADIR MODULE

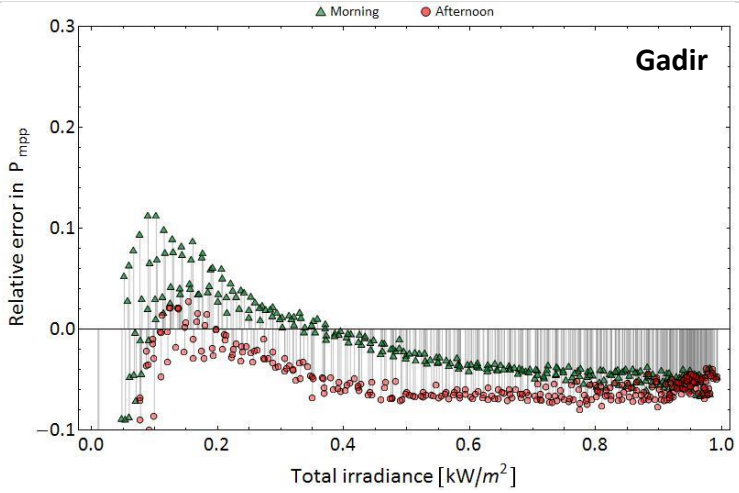

Figure 23 Relative modeling error in P_{mpp} for the Gadir module, with total irradiance (G) and module temperature (T) as model inputs.

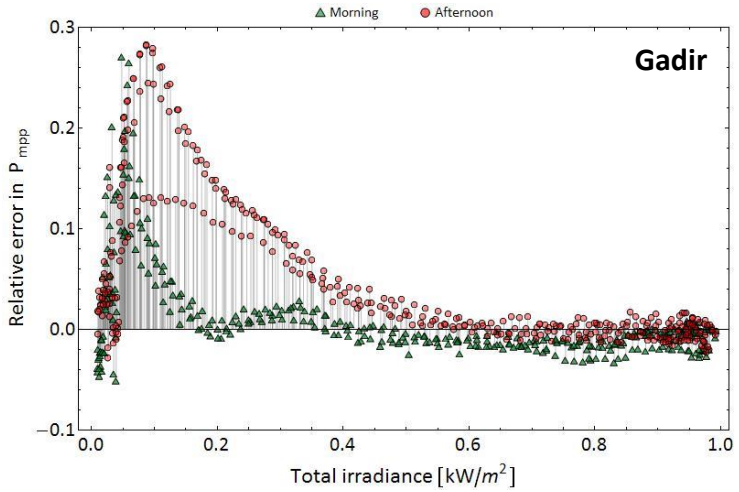

Figure 24 Relative modeling error in P_{mpp} for the Gadir module, with useful irradiance (UI) and module temperature (T) as model inputs.

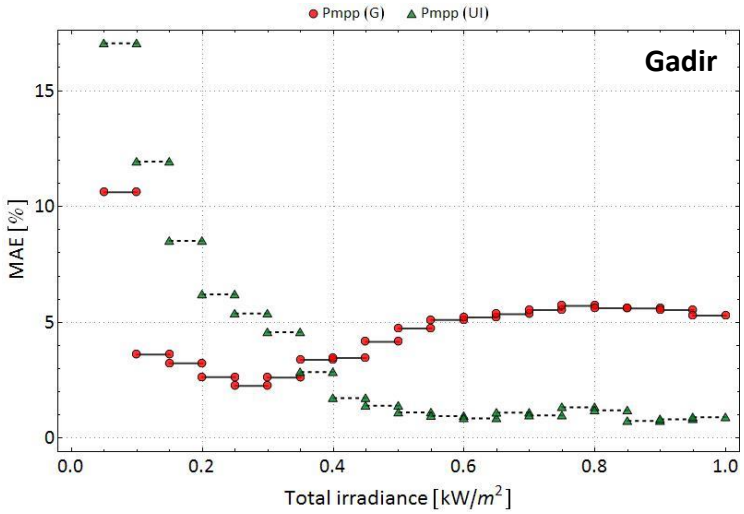

Figure 25 Mean absolute modeling error in P_{mpp} for the Gadir module on clear days in July on a 50 W/m² irradiance interval.

6.2.2.2. FLEXCELL MODULE

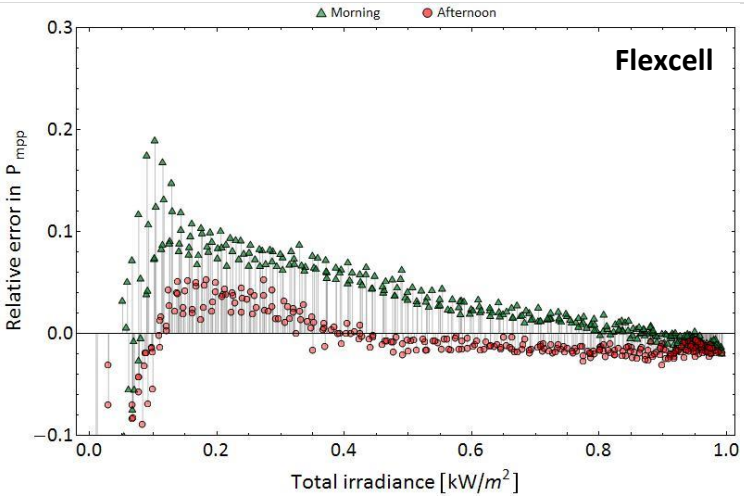

Figure 26 Relative modeling error in P_{mpp} for the Flexcell module, with total irradiance (G) and module temperature (T) as model inputs.

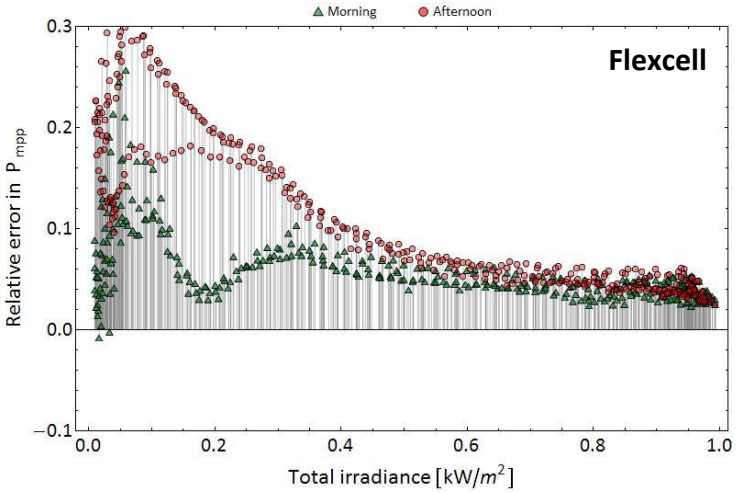

Figure 27 Relative modeling error in P_{mpp} for the Flexcell module, with useful irradiance (UI) and module temperature (T) as model inputs.

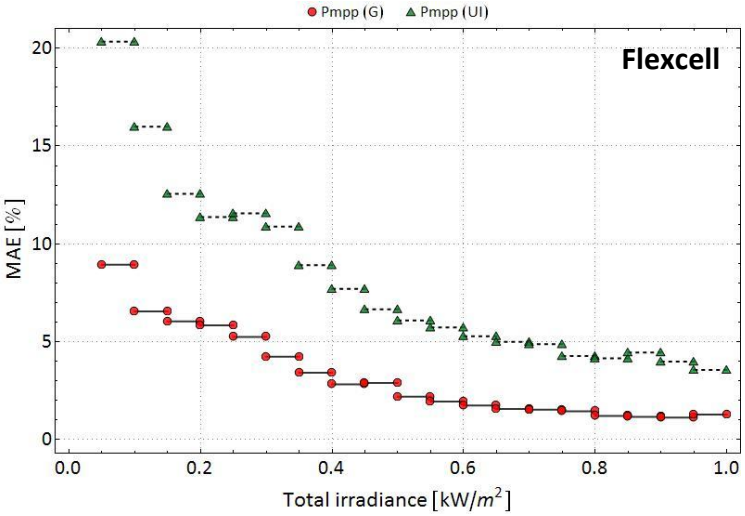

Figure 28 Mean absolute modeling error in P_{mpp} for the Flexcell module on clear days in July on a 50 W/m² irradiance interval.

6.2.2.3. CONCLUSIONS

A-Si panels are expected to be most sensitive to spectral effects. The useful irradiance is a first order approximation to account for changes in the spectral distribution. Modeling the P_{mpp} for Gadir shows that with UI the model improves significantly for $G > 0.35\ kW/m^2$. The morning-afternoon discrepancy is reduced when regarding the useful irradiance. However again, low modeling accuracy is observed for low irradiation values ($G < 0.2\ kW/m^2$).

Figure 28 shows that the Flexcell model does not improve under replacing G by the useful irradiance. Under high irradiation, the MAE of the modeled power with UI as input increases by approximately 3-5%-points. Similar to the other modules, the large error at low irradiance remains.

The difference observed between the Gadir and Flexcell a-Si panels might originate from the rough definition of the useful irradiance. Among different a-Si modules the semiconductor material and thus the band gap differs slightly and consequently the spectral response is different. The fraction of irradiance that is considered useful therefore varies per module. By defining the range of the UI between 350 and 780 nm, implicitly it is assumed that all a-Si modules are sensitive to the same range of irradiance. The modeling difference between the Gadir and Flexcell modules shows that this assumption might be wrong. A more specific definition of the useful irradiance would require more information on the specific band gap of the material.

6.3. AVERAGE PHOTON ENERGY

Resemblance between all four models is found in the overestimation of P_{mpp}[15] at low incident irradiance. Apparently, these spectra contain less useful irradiance than anticipated by the model, even when accounting for changes in the spectral distribution by means of the useful irradiance. Observing Figure 9 shows that low irradiance spectra on clear days are characterized by higher average photon energy than high irradiance spectra, which are characterized by an approximately constant APE of $\sim 1.90\ eV$. Moreover, the spectral response curves shown in Figure 3 demonstrate that high energy photons are absorbed with decreasing energy efficiency. High energy photons induce equal current as an equal amount of low energy photons. The excess energy is lost and thus energy efficiency is decreased. For the same total irradiance a blue rich spectrum (high APE) is thus expected to have lower power output than a red-rich spectrum (low APE). The UI does not capture this effect, since it is related to the EQE and does not contain information on energy efficiency.

The effect of the APE on the P_{mpp} is further investigated by Pearson's correlation coefficient, a built-in Mathematica 8 function:

$$r = \frac{\sum_{i=1}^{n}[x_i - \bar{x}][y_i - \bar{y}]}{\sigma_x \sigma_y (n-1)}$$

Here, σ_x and $\bar{x}$ are the standard deviation and the mean of variable x respectively. Using this relation, correlation between the P_{mpp} and the APE for different data point-intervals was computed. Figure 29 shows that correlation is strong and negative, i.e. deviation from the mean is negative for P_{mpp} while being positive for APE or vice versa, for low irradiance values ($\sim 80 - 250\ W/m^2$). Note that the total irradiance and useful irradiance for the four clear days are uniquely characterized by a single value of the APE. Consequently similar correlation is observed for P_{mpp} vs G and P_{mpp} vs UI. The relation as proposed by (Betts, 2004) in equation 10 was investigated between the normalized temperature

[15] The same holds for the short circuit current, since I_{sc} and P_{mpp} are strongly correlated.

corrected current response and the APE. It should in particular correct the short circuit current under low irradiance, i.e. high APE. Figure 30 shows that for $APE > 1.90\ eV$ the data has a wide distribution. Hence, a simple relation obtained by least-squares fitting will not make sense; whereas the APE reveals a change in spectral irradiance for the low irradiance regime, there is no simple relation that allows one to correct the PV performance for these changes.

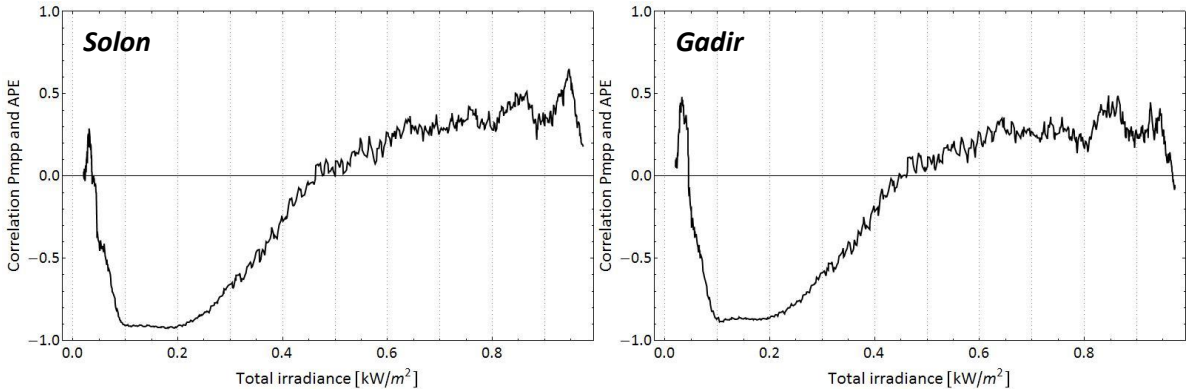

Figure 29 Correlation between power output and average photon energy for Solon and Gadir. Both modules show strong negative correlation for total irradiance between ~180-250 W/m².

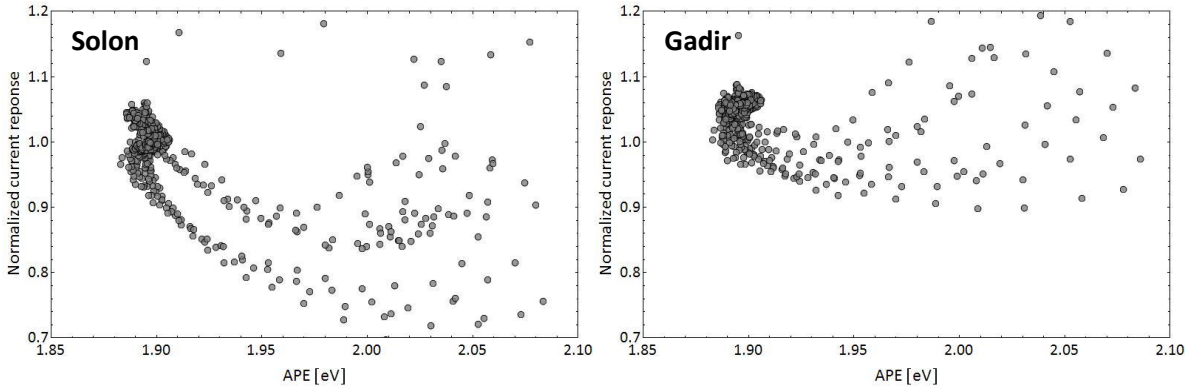

Figure 30 Normalized, temperature corrected current response versus average photon energy for Solon and Gadir. Especially for higher APE, there is no simple relation that fits these data points.

6.4. SUMMARY OF RESULTS

6.4.1. CRYSTALLINE-SILICON

Figure 31 and Figure 32 show the modeling accuracy of the empirical model compared to the simple two-diode model benchmark of the Solon and BP module respectively. It follows that the Solon panel is modeled by both approaches with similar accuracy, $MAE_{G=0.3-1.0\ kW/m^2} \approx 5-1\%$. For the BP module, the empirical model yields better modeling accuracy, by several %-points.

Despite that accounting for spectral effects by inclusion of the UI significantly reduces the modeling discrepancy between morning and afternoon, only slight improvement in the intermediate irradiance range and deterioration in the high irradiance regime is observed. This stresses the small influence spectral effects have on c-Si module performance modeling. Overall, for similar modeling accuracy, the two-diode model is more practical, as no measurements are needed to calibrate the model.

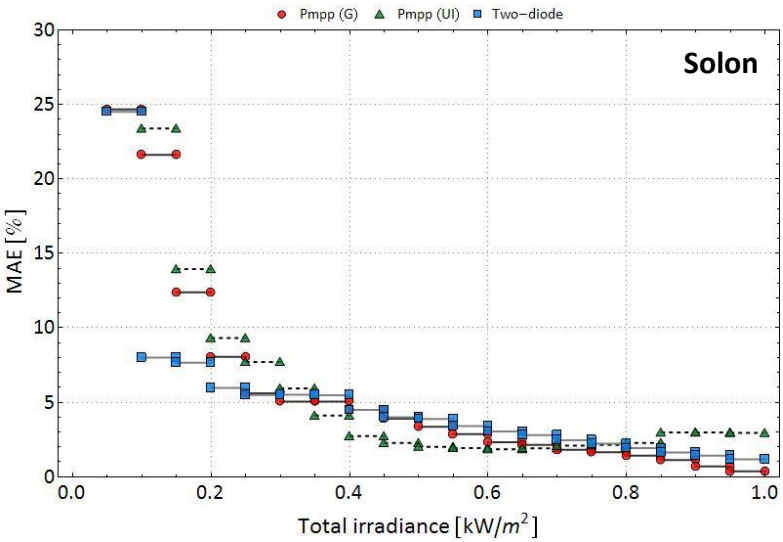

Figure 31 Inter-comparison of the mean absolute error of the simple two-diode model (blue squares) and the empirical model (red disks and green triangles) for the Solon module.

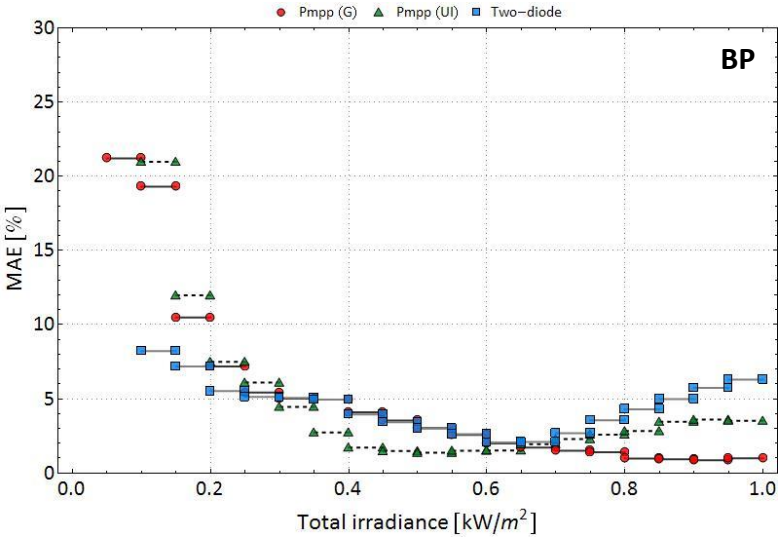

Figure 32 Inter-comparison of the mean absolute error of the simple two-diode model (blue squares) and the empirical model (red circles and green triangles) for the BP module.

6.4.2. AMORPHOUS-SILICON

Accounting for spectral effects by means of the useful irradiance improves especially the Gadir a-Si modeling accuracy (Figure 33), mainly for $G < 0.6\ kW/m^2$. Compared to the two-diode benchmark, modeling error is reduced significantly to $MAE_{G=0.3-1.0\ kW/m^2} \approx 3-1\%$, which is even better than the conventional modeling accuracy for c-Si modules. The Flexcell (Figure 34) module lacks a two-diode reference model and moreover, does not improve upon inclusion of the useful irradiance, possibly due to a mismatch between the range of the modeled and realistic useful irradiance. However, the empirical modeling accuracy with total irradiance as input is similar to that of the c-Si modules, $MAE_{G=0.3-1.0\ kW/m^2} \approx 4-1\%$.

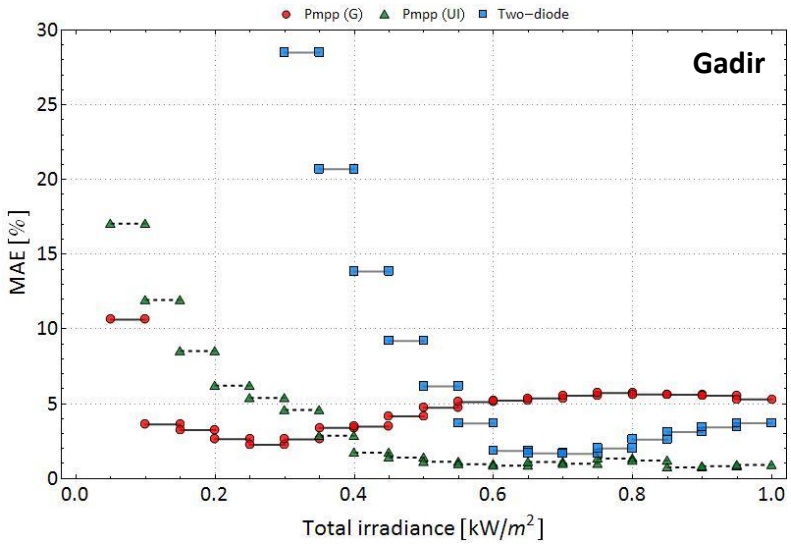

Figure 33 Inter-comparison of the mean absolute error of the simple two-diode model (blue squares) and the empirical model (red circles and green triangles) for the Gadir module.

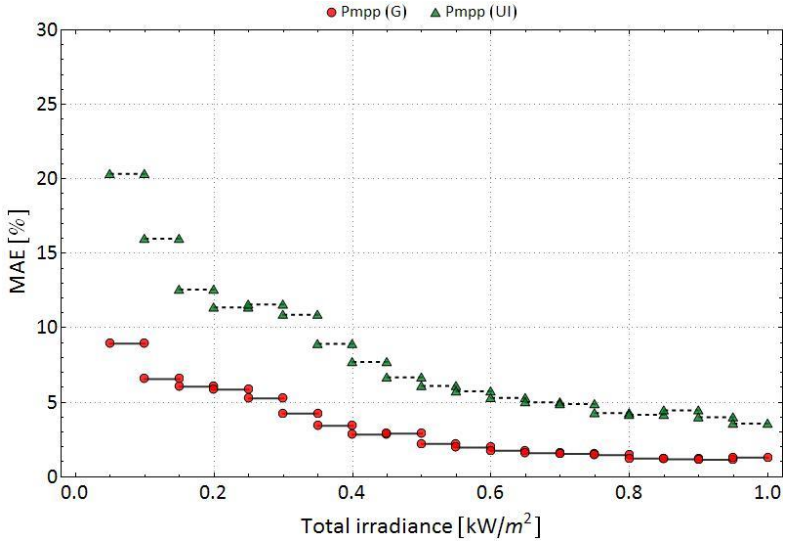

Figure 34 Mean absolute error of the empirical model (red circles and green triangles) for the Flexcell module.

6.4.3. AVERAGE PHOTON ENERGY

Overall, the empirical model on clear days is inaccurate under low irradiance ($G < 0.3\ kW/m^2$), which comprises 35% of the data points on the days studied[16]. An increase in APE, caused by light scattering at high air mass enhancing blue diffuse irradiance, reveals a change in spectral distribution here, but a simple relation, such as equation 10, is unable to correct for these changes. This might either be caused by the fact that the APE does not fully describe the spectral quality of the light or that taking only clear days does not fully reveal this relation.

[16] Of course, on clouded days occurrence of low irradiance is even higher; however the results discussed here were not examined for clouded days.

7. CONCLUSIONS

7.1. SPECTRAL IRRADIANCE CHARACTERIZATIONS

Three spectral irradiance characterization methods are presented, the total irradiance, useful irradiance and average photon energy in order to monitor and reveal changes in the spectral irradiance. On clear days, PV module performance as a function of total irradiance displays a discrepancy between morning and afternoon. The device itself does not change throughout the day, and hence this indeed is caused by a change in spectral irradiance, which is not fully captured by the total irradiance. The spectral effects on PV performance stress that the total irradiance is not sufficient for characterization of the incident irradiance for PV performance modeling.

The useful irradiance does distinguish between morning and afternoon and is therefore more suitable for characterizing the spectral irradiance. Besides, the APE reveals that at low incident irradiance, the spectrum is blue shifted as a result of high air mass, which is not captured by the useful irradiance; The APE, however, does not contain information on the total energy content of the incident irradiance and is therefore to be used in combination with either the useful or total irradiance.

7.2. ACCOUNTING FOR VARIATIONS IN THE SPECTRAL IRRADIANCE DISTRIBUTION

Spectral effects have only a small effect on crystalline-silicon panels and can therefore be neglected in c-Si PV performance modeling. Of the three spectral parameterization methods investigated, the useful irradiance shows best results in accommodating the spectral irradiance on clear days; accounting for variations in the spectral irradiance by means of the useful irradiance, the modeling accuracy for amorphous-silicon modules can be improved significantly, as demonstrated for the Gadir module. However, this modeling approach is inconsistent when there is a mismatch between the EQE approximated by the useful irradiance and the actual EQE of the module, as demonstrated for the Flexcell module.

Low modeling accuracy is obtained at low incident irradiance, which is caused by a blue shift of the spectrum that is not captured by the useful irradiance. The average photon reveals these changes; nevertheless on clear days, a simple relation between module performance and APE to correct for these spectral changes was not found. Improving PV performance modeling under low irradiance remains a challenge and requires more comprehensive characterizations of the spectral irradiance than the average photon energy and useful irradiance.

8. DISCUSSION

This research was carried out on clear days only and is therefore not fully representative for outdoor conditions. Clouded days will exhibit additional shading and scattering effects and corresponding changes in PV performance. Nonetheless, the smooth irradiance variations on clear days allow one to study spectral effects on performance under controlled outdoor conditions where these effects are not present. Knowledge obtained for clear days, can then be extended to clouded days in a similar framework of that presented in this report.

Experimental limitations have caused adjustment of the lower limit of the useful irradiance, from 300 to 350 nm. Because the useful irradiance is roughly defined, this adjustment is expected to have little effects on the conclusions drawn here. Additionally, the spectral response in this region is small and

irradiance within this interval does only contribute marginally to the photo current. Finally, the empirical relation between the power at the maximum power point and the short circuit current proposed by (Beyer, Yordanov, Midtgard, Saetre, & Imenes, 2011) requires least-squares fitting. The sensitivity of the fitting-parameters on the day of calibration is not investigated here. It would be an idea for future research to perform a sensitivity analysis on the modeled PV performance throughout the year under Dutch environmental conditions, to investigate the effect of the calibration day.

9. RECOMMENDATIONS

In the framework of the effects of spectral distribution on PV performance, a few recommendations can be made for future research.

Firstly the study could be extended to include clouded days. Shading by clouds, however, makes interpretation of the data acquired by the experimental setup more complicated. It should be checked whether the I-V curve is a result of a single set of environmental conditions, which is not disturbed by shading. Composite I-V curves, resulting from long I-V measurements, should be avoided by utilizing fast I-V curve tracers such as the MP-160 device used here. In cases composite faulty I-V curve do exist, these can be rejected from the data by allowing only a few % variation in the irradiance during an I-V measurement.

Secondly, more comprehensive spectral characterization parameters or extensions to existing methods could be investigated. Especially for the low irradiance range, these parameters should be sensitive to changes in the spectral irradiance. For example, the useful irradiance could be improved by including module specific parameters or by accounting for energy efficiency instead of quantum efficiency only. Furthermore a relation between the APE and Pmpp or Isc could be checked for clouded days, which might have not been apparent from examining clear days only.

Thirdly, one could study multi-junction devices, which are expected to be even more sensitive to the spectral irradiance distribution. A correction for the useful fraction for multi-junction solar cells is proposed in (Beyer, Gottschalg, Betts, & Infield, 2003), but due to absence of experimental data on multi-junction cells this relation was not studied in this research project.

Finally, performing a sensitivity analysis for the power at the maximum point versus the calibration day in the year would provide information on how the modeling accuracy varies during the year.

Of course, the manufacturer could also contribute to improving outdoor PV performance modeling. Either by providing additional performance data under different incident spectra, or even more by providing the spectral response of the module.

WORKS CITED

Badescu, V., Gueymard, C., S., C., Oprea, C., Baciu, M., Dumitrescu, A., . . . Rada, C. (2012). Computing global and diffuse solar hourly irradiation on clear sky. Review and testing of 54 models. *Renewable and Sustainable Energy Reviews 16*, 1636-1656.

Betts, T. (2004). *Doctoral thesis: Investigation of Photovoltaic Device Operation under Varying Spectral Conditions.* Loughborough University.

Beyer, H., Gottschalg, R., Betts, T., & Infield, D. (2003). Modelling the realistic short circuit current and mpp power of A-SI single and multijunction devices. *Proceedings of the 3rd World Conference on Photovoltaic Energy Conversion*, (pp. 2435-2438). Osaka.

Beyer, H., Yordanov, G., Midtgard, O.-M., Saetre, T., & Imenes, A. (2011). Contributions to the knowledge base on PV performance: Evaluation of the operation of PV systems using different technologies installed in southern Norway. *37th IEEE Photovoltaic Specialists Conference*, (pp. 3103-3108). Seattle.

Bird, R., & Riordan, C. (1986). Simple solar spectral model for direct and diffuse irradiance on horizontal and tilted planes at the earth's surface for cloudless atmospheres. *Journal of Climate & Applied Meteorology 25*, 87-97.

Chih-Tang, S., Noyce, R., & Shockley, W. (1957). Carrier Generation and Recombination in P-N Junctions and P-N Junction Characteristics. *Proceedings of the IRE 45*, (pp. 1228 - 1243).

Demain, C., Journée, M., & Bertrand, C. (2012). Evaluation of different models to estimate the global solar radiation on inclined surfaces. *Renewable Energy 50*, 710-721.

Emery, K. (1986). Solar simulators and I-V measurement methods. *Solar Cells 18*, 251-260.

Emery, K. (2012, 06 19). *Reference AM 1.5 spectra.* Retrieved 11 5, 2012, from NREL: http://rredc.nrel.gov/solar/spectra/am1.5/

Gottschalg, R., Betts, T., Infield, D., & Kearney, M. (2004). On the importance of considering the incident spectrum when measuring the outdoor performance of amorphous silicon photovoltaic devices. *Measurement Science and Technology 15*, 460–466.

Gottschalg, R., Betts, T., Infield, D., & Kearney, M. (2005). The effect of spectral variations on the performance parameters of single and double junction amorphous silicon solar cells. *Solar Energy Materials & Solar Cells 85*, 415–428.

Gueymard, C. (2001). Parameterized transmittance model for direct beam and circumsolar spectral irradiance. *Solar Energy 71*, 325-346.

Hoff, T., & Perez, R. (2012). Modeling PV fleet output variability. *Solar Energy 86*, 2177-2189.

Ishaque, K., Salam, Z., & Syafaruddin. (2011). A comprehensive MATLAB Simulink PV system simulator with partial shading capability based on two-diode model. *Solar Energy 85*, 2217-2227.

Ishaque, K., Salam, Z., & Taheri, H. (2011). Simple, fast and accurate two-diode model for photovoltaic modules. *Solar Energy Materials & Solar Cells 95*, 586-594.

Kate, M. (2012, juli 02). Kate, M. t. (2012, 07 02). IQE curves.

Krishnan, P., Schüttauf, J., van der Werf, C., Houshyani Hassanzadeh, B., van Sark, W., Schropp, R., & e, 2. (2009). Response to Simulated Typical Daily Outdoor Irradiation Conditions of Thin Film Silicon Based Triple Band Gap, Triple Junction Solar Cells. *Solar Energy Materials and Solar cells 93*, 691-697.

Los, A. (2012). *EKO Instruments Europe.* Retrieved January 18, 2012, from www.eko-eu.com: http://eko-eu.com/files/EKO-MP160-12-09E-NH.pdf

Minemoto, T., Toda, M., Nagae, S., Gotoh, M., Nakajima, A., Yamamoto, K., . . . Hamakawa, Y. (2007). Effect of spectral irradiance distribution on the outdoor performance of amorphous Si/thin-film crystalline Si stacked photovoltaic modules. *Solar Energy Materials and Solar Cells 91*, 120-122.

Myers, D. (2012). Direct beam and hemispherical terrestrial solar spectral distributions derived from broadband hourly solar radiation data. *Solar Energy 86*, 2771-2782.

Twidell, J., & Weir, T. (2006). *Renewable energy resources.* New York: Taylor & Francis Ltd.

van Sark, W., Louwen, A., de Waal, A., Elsinga, B., & Schropp, R. (2012). UPOT: the Utrecht photovoltaic outdoor test facility.

Williams, S., Betts, T., Helf, T., Gottschalg, R., Beyer, H., & Infield, D. (2003). Modeling long-term module performance based on realistic reporting conditions with conderation to spectral effects. *Proceedings of the Third World Conference on Photovoltaic Energy Conversion*, (pp. 1908–1911). Osaka, Japan.

Willmott, C., & Matsuura, K. (2005). Advantages of the mean absolute error (MAE) over the root mean square error (RMSE) in assessing average model performance. *Climate Research 30*, 79–82.

APPENDIX

I. INTERMEDIATE RESULTS: SIMPLE TWO-DIODE MODEL

Modeling P_{mpp} using the simple two-diode model requires computation of the series and shunt resistance. For this, the I-V and P-V characteristics under standard test conditions are reproduced, which are shown in Figure 35. The associated R_s and R_p are displayed in Table 4.

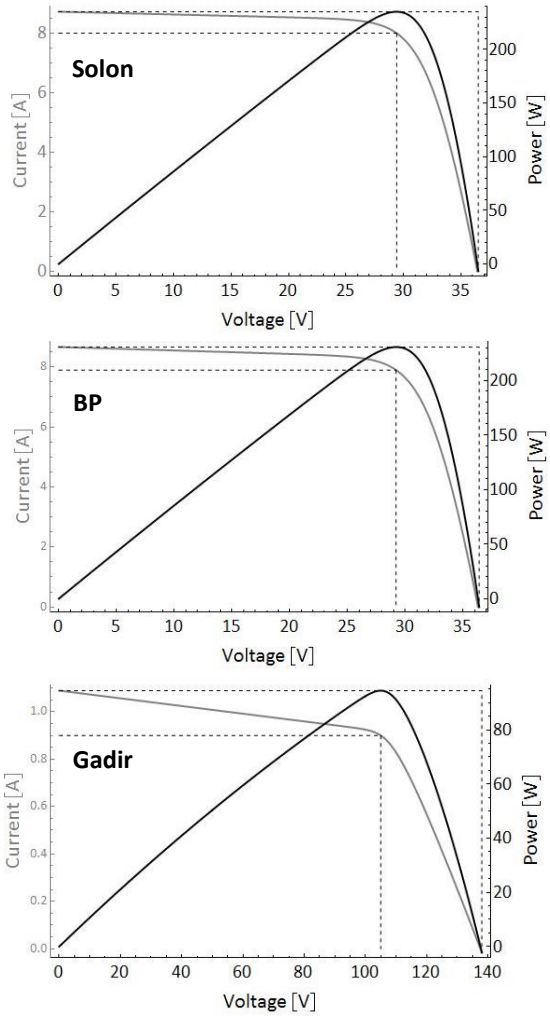

Figure 35 Modeled current-voltage (gray, left axis) and power-voltage characteristics (black, right axis) under STC for the Solon, BP and the Gadir module respectively. The inner dashed lines indicate the I_{mpp} and V_{mpp}, whereas the outer dashed lines indicate I_{sc}, and V_{oc}.

Table 4 Modeled series and shunt resistance R_s and R_p.

Module	R_s [Ω]	R_p [Ω]
Solon	0.32	107
BP	0.33	86.6
Gadir	27.5	589

II. INTERMEDIATE RESULTS: EMPIRICAL MODEL

In this research the mean absolute error was used to quantify the modeling accuracy, whereas in literature, commonly the root mean squared error and mean bias error are used. For inter-comparison between this report and other literature, the RMSE and MBE are shown below. Additionally, the fitting procedure (equation 11) for the power at the maximum power points is included for the BP, Gadir and Flexcell modules.

II.I. SOLON

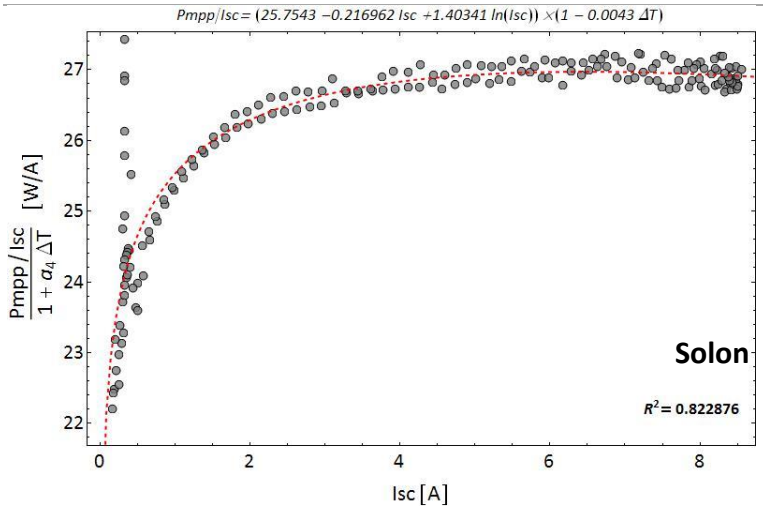

Figure 36 Power-current response least-squares fit (equation 11) on July 23 for the Solon module.

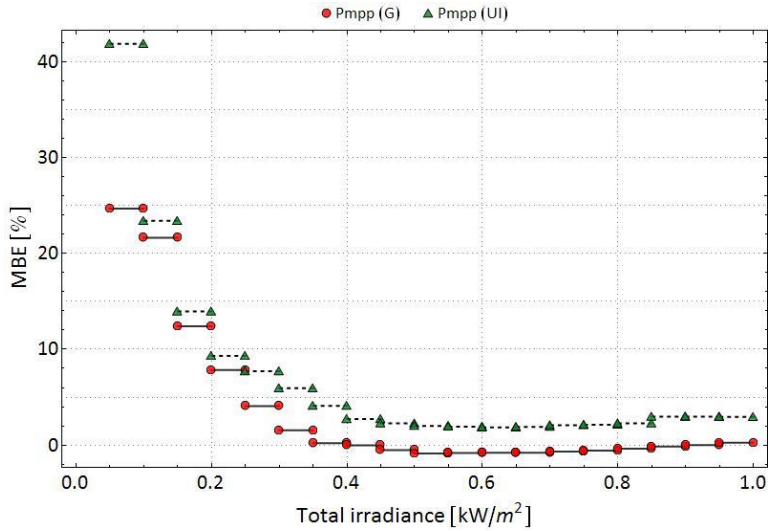

Figure 37 Mean bias error in P_{mpp} for the Solon module on clear days in July on a 50 W/m² irradiance interval.

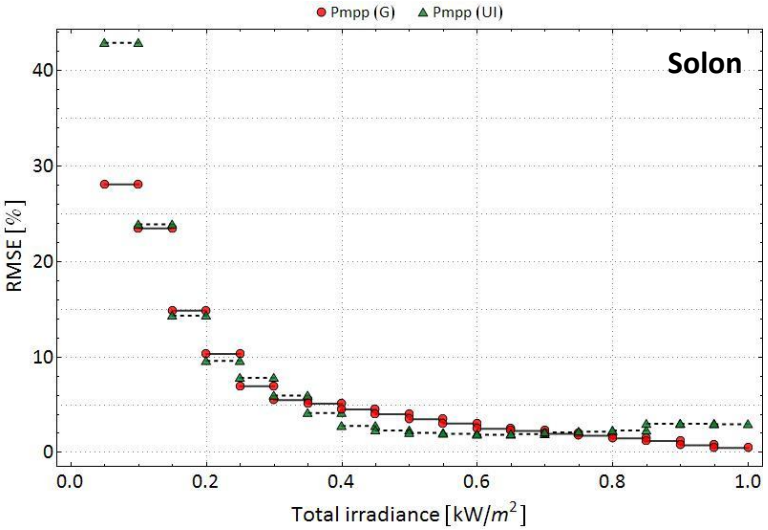

Figure 38 Root mean squared error in P_{mpp} for the Solon module on clear days in July on a 50 W/m² irradiance interval.

II.II. BP

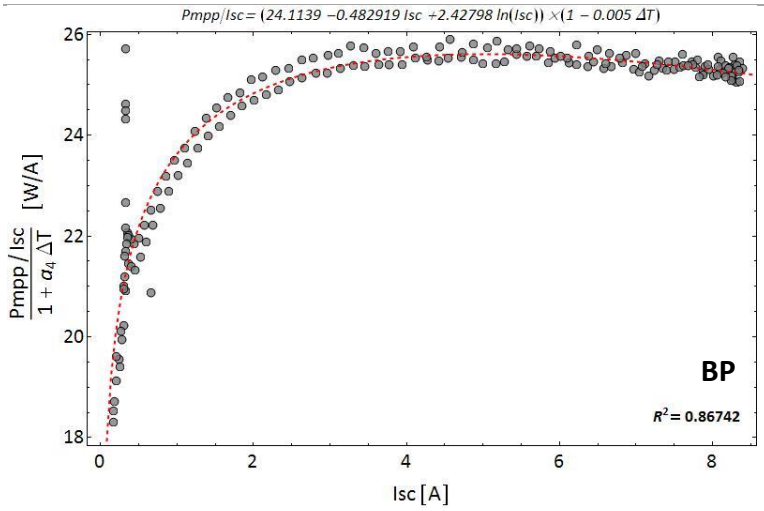

Figure 39 Power-current response least-squares fit (equation 11) on July 23 for the BP module.

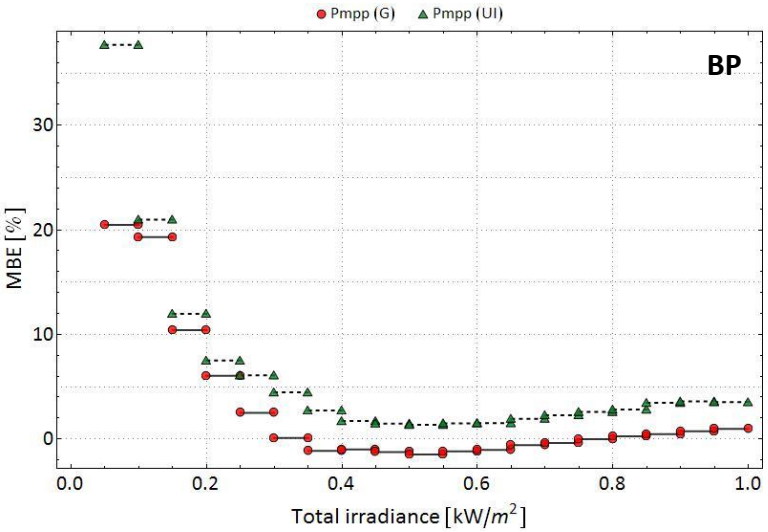

Figure 40 Mean bias error in P_{mpp} for the BP module on clear days in July on a 50 W/m² irradiance interval.

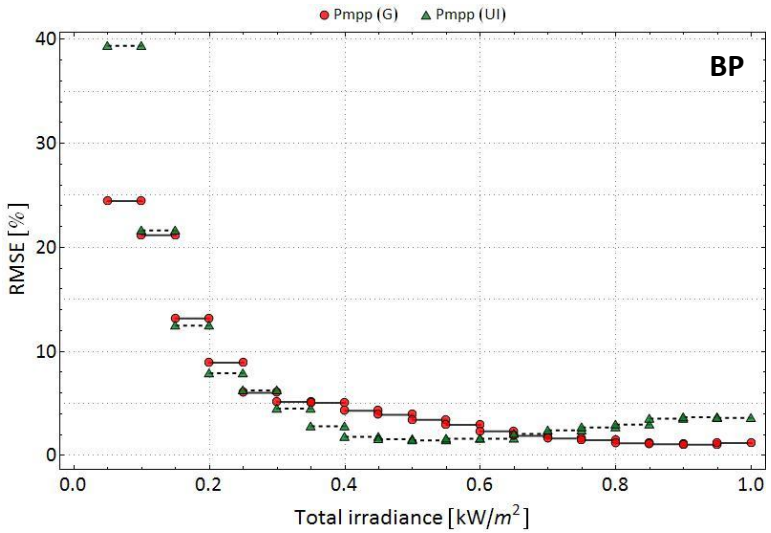

Figure 41 Root mean squared error in P_{mpp} for the BP module on clear days in July on a 50 W/m² irradiance interval.

II.III. GADIR

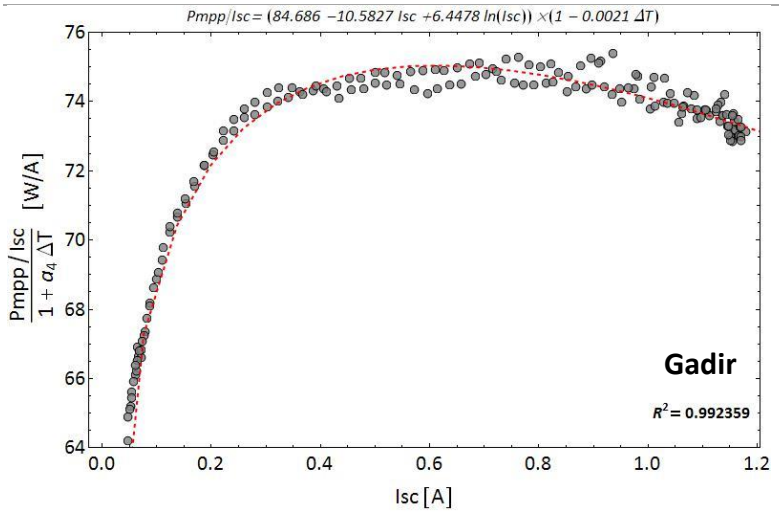

Figure 42 Power-current response least-squares fit (equation 11) on July 23 for the Gadir module.

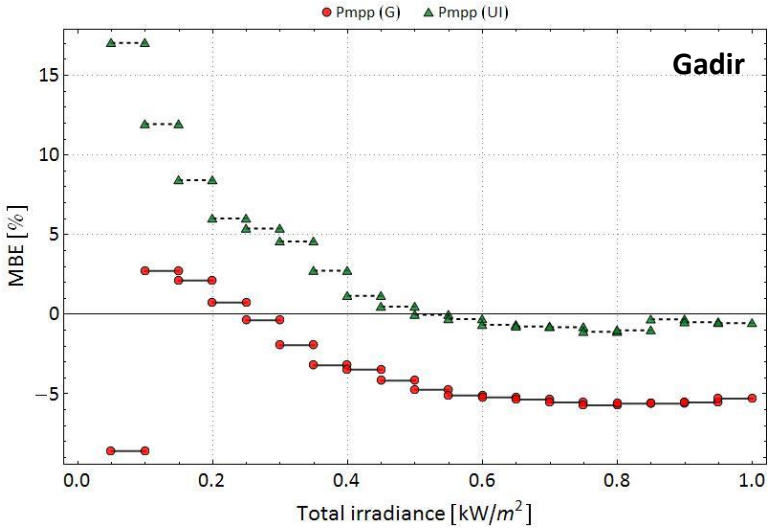

Figure 43 Mean bias error in P_{mpp} for the Gadir module on clear days in July on a 50 W/m² irradiance interval.

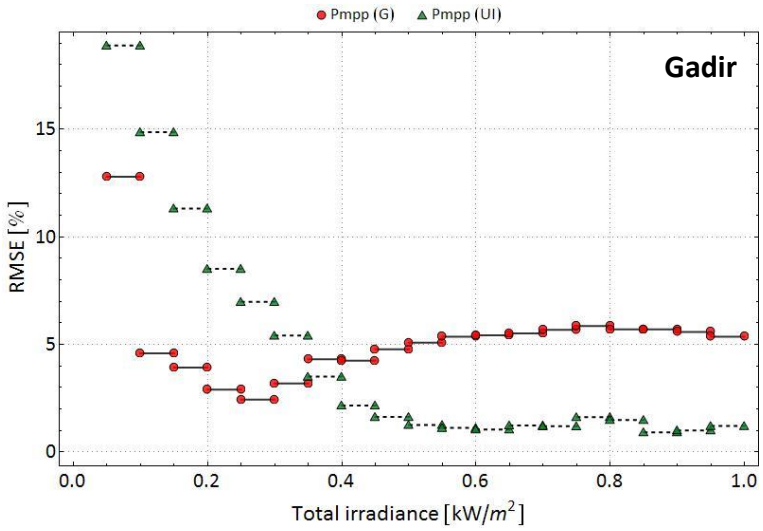

Figure 44 Root mean squared error in P_{mpp} for the Gadir module on clear days in July on a 50 W/m² irradiance interval.

II.IV. FLEXCELL

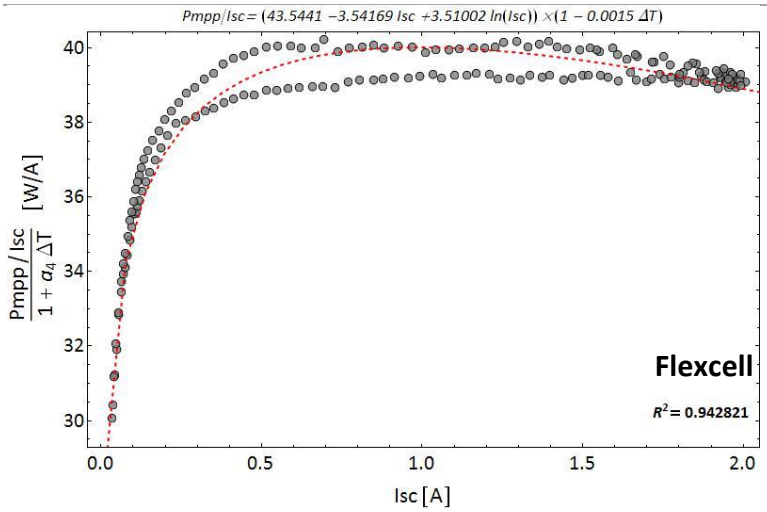

Figure 45 Power-current response least-squares fit (equation 11) on July 23 for the Flexcell module.

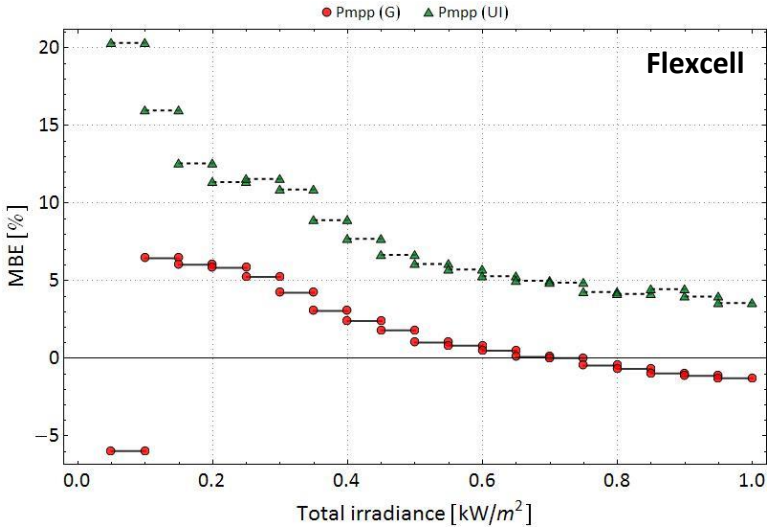

Figure 46 Mean bias error error in P_{mpp} for the Flexcell module on clear days in July on a 50 W/m² irradiance interval.

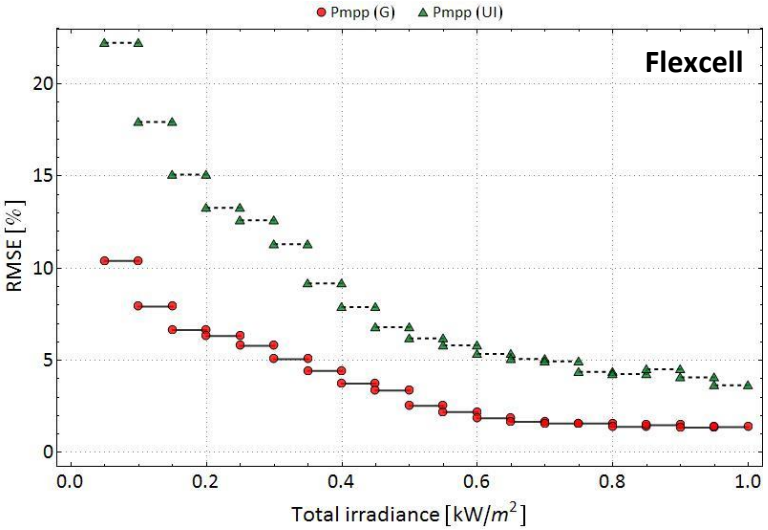

Figure 47 Root mean squared error in P_{mpp} for the Flexcell module on clear days in July on a 50 W/m^2 irradiance interval.